The effect of uncertainty in composition on Laser-Induced Grating thermometry.

Megan Edwards

MSc Thesis

Department of Atomic and Laser Physics,

Clarendon Laboratory,

University of Oxford.

The effect of uncertainty in composition on Laser-Induced Grating thermometry.

Megan Edwards, Lady Margaret Hall, MSc by Research, Trinity 2011.

Abstract

The effect of uncertainty in gas composition on the accuracy of gas-phase thermometry using Laser-Induced Thermal Grating Spectroscopy, LITGS, is studied. Temperatures are obtained from measurements of the sound speed derived from the frequency of oscillations f_{osc}, imposed upon the LITGS signal arising from the transit of acoustic waves across the density modulation feature. The dependence of the sound speed, c_s on $\sqrt{\gamma/m}$, where γ is the ratio of specific heats and m is the mean molecular mass leads to a dependence upon gas composition.

LITGS signals were generated in acetone vapour in a variety of gas mixtures in a temperature controlled cell at 4 bar total pressure using pump pulses from a frequency quadrupled Q-switched Nd:YAG laser at 266 nm and a cw diode pumped solid state probe laser at 671 nm. Studies were undertaken of the variation in f_{osc} with gas composition using gas mixtures of O_2 and N_2 with component concentrations in the range 0-100 %, and was found to agree with theoretical predictions. Measurement precision of the data (one standard deviation in 50 measurements) was found to be typically $\pm$ 1.7 % for measurements at 4 bar total pressure.

The effect of varying concentrations in exhaust gas residuals (EGR) typical of pre-ignition gases in a spark ignition internal combustion engine were studied using synthetic air (N_2/ O_2 mixtures) containing variable amounts of simulated EGR components, CO_2 and H_2O. The effect of variation in CO_2 concentration in dry synthetic air was measured at 4 bar and 30°C and found to agree with theoretical predictions. Experiments conducted at 30°C, with the addition of a saturated vapour pressure of water indicate that the effect of a saturated vapour pressure of water on

the oscillation frequency in synthetic EGR is on the borderline of resolution.

The effect of variable amounts of typical hydrocarbon fuel vapour on f_{osc} was studied using 2,2,4-trimethyl-pentane in gas mixtures composed of synthetic air and variable amounts of EGR and water vapour at 80°C.

Kinetic theory was used in order to model the dependence of f_{osc} on various gas compositions containing fuel and EGR, in order to construct an error surface for comparison with experimental measurements. Experimental data were found to agree with the model predictions to within experimental error for a representative data set within the range of calculated values. The results indicate that uncertainties in temperature values derived from LITGS thermometry can be estimated with confidence within reasonable estimates of composition variations in an internal combustion engine, and should lead to absolute temperature accuracy of within 2-3 %.

Acknowledgements

There are certain people who have made this work possible, and some without whom the experience would have been a much lesser one.

Firstly, my supervisor Professor Paul Ewart gave me the opportunity to work in his group and to follow my career aspirations. His enthusiasm, attentive supervision and great kindness are very much appreciated. Great recognition goes to Dr. Ben Williams for his friendship, his ability and willingness to teach me so much and for his seemingly unending patience with my equally unending avalanche of questions. Thanks to the rest of the group; Dr. Michelle Hamilton, Alex Thompson and Henry Northern for helping to make the working environment a pleasant one.

I would like to take this opportunity to thank Dr. Natasa Vasiljevic and Dr. Terry McMaster at the University of Bristol; the former, for her kindness, continued support and enthusiasm and the latter for not only all of the above qualities but also for giving me the invaluable opportunity to study physics in the first place.

A number of other people have been highly instrumental in outweighing the downsides of my time in Oxford whilst probably not quite realising the extent to which this is true. They are; Holly Morse, Andrew Joseph, Emily Popp, Alice Cresswell, Charles Finch, Ceri Brenner, Chris Compton, Julia Shanks, William Lawrance, Tom Jenkins, Hannah Mays, James Sinclair, Helen Batchelor, Natalie Sanderson and Sean O'Reilly; a group of people who, in my experience, have an understanding of each other that is deeper than most.

Lastly, and by absolutely no means least, I would like to extend my thanks to my family for tolerating my most socially reclusive year to date. To Carol and Raymond Ford for the haven of kindness that they have always afforded me, and to Pauline and Stan Edwards for the inspiration that they provide. Particular thanks to my parents, Peter and Paula Edwards, for their unfailing support, the conversations and their visits to Oxford which made, quite literally, all of the difference.

For my parents, Peter and Paula Edwards.

Contents

Nomenclature: Acronyms and Constants

For clarity, the names of a number of scientific processes, concepts and devices have been shortened to acronyms within the text. These are listed in the table below.

Acronym	Meaning
LITGS	Laser-Induced Thermal Grating Spectroscopy
CARS	Coherent anti-Stokes Raman Spectroscopy
UV	Ultra Violet
cw	Continuous wave
IC	Internal Combustion (engine)
PMT	Photomultiplier tube
DPSSL	Diode pumped solid state laser
EGR	Exhaust gas residual
Nd:YAG	Neodymium-doped yttrium aluminium garnet
LIF	Laser-Induced Fluorescence
FWHM	Full width, half maximum
FWM	Four-wave mixing
DFWM	Degenerate four-wave mixing

Table 1: Acronyms and Abbreviations

Chapter 1

Introduction

1.1 The motivation to study combustion

The efficient use of available energy reserves is arguably one of the greatest current challenges for science and technology. The accessible sources of fossil fuels on which we are dependent are decreasing at a significant rate relative to the estimated reserves [1]. Ultimately, in order to maintain our way of life, alternative energy sources must be found [2, 3]. Until an alternative method of energy production is widely implemented, however, the combustion of fossil fuels will remain essential to our society. In particular, the efficient extraction of energy from fuel is an important consideration for internal combustion engines. Increasing pressure from both consumers and legislation to improve efficiency and reduce emissions calls for further research into combustion processes [4].

The ability to measure fundamental physical parameters during combustion is of great importance. Specifically, temperature is an important parameter in determining the performance of heat engines and is also a critical factor in the rate of many chemical reactions involved in combustion. Understanding of the complex interplay between temperature and component design is required to support further evolution

and innovation of IC engines in order to improve performance and efficiency.

Various methods can be used to measure temperature within IC engines, of both traditional (non-optical) and optical nature. An example of a traditional diagnostic method is the thermocouple, which has the disadvantage that it is invasive; in order to make a measurement, it is necessary to insert a probe into the environment under investigation. This can render the measurement inaccurate owing to a tendency to conduct heat away from the measurement location; in addition, physical probes are undesirable for gas measurements since they perturb flow. Optical methods provide an attractive alternative; in general, lasers can provide a non-perturbative and non-invasive probe. Provided that optical access to the measurement region is available, optical methods can yield measurements of fundamental parameters such as temperature without interfering with the properties of the system under investigation.

The focus of this work is the measurement of temperature within pre-combustion gas mixtures, using the method of Laser Induced Thermal Grating Spectroscopy (LITGS). The accuracy and precision of LITGS thermometry is dependent upon fluctuations in gas composition. This work will present a systematic study of the effect of the uncertainty in gas composition on LITGS measurements.

1.2 Laser-Induced Grating Spectroscopy

A laser-induced grating (LIG) is produced by the interference of two laser beams. For the case of thermal gratings, heating by the process of quenching, largely due to collisions, occurs following molecular excitation of the gas vapour by the pump beams when the beams have a frequency corresponding to a resonance in the gas species. This results in rapid, localised heating in the regions of high intensity within the interference pattern. The interference of the two beams thus produces a spatial

variation in the density of the gas in the crossing region.

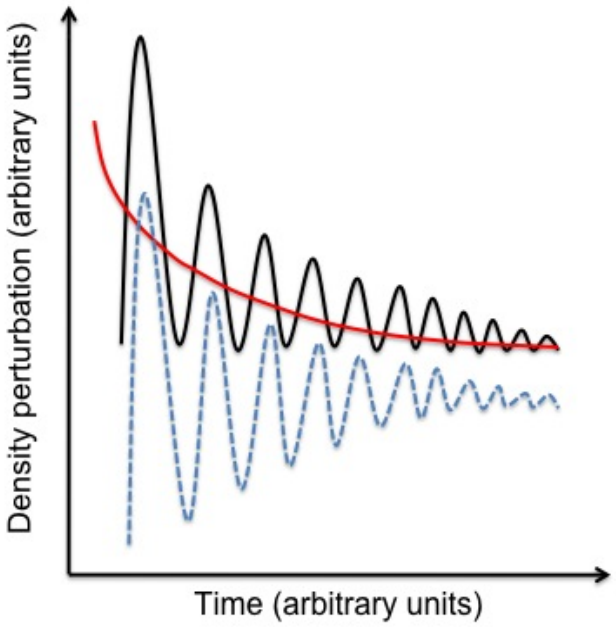

Figure 1.1: *The total density perturbation (black oscillating line) has two contributions; a stationary temperature grating (red exponentially decaying curve) and an acoustic pressure perturbation (blue dashed oscillation).*

There are two contributions to the overall grating; the temperature component and a pressure component. As a result of the rapid heat deposition and corresponding density modulation an acoustic wave is initiated, which travels perpendicular to the grating planes in either direction originating from regions of high intensity within the interference pattern. These counter-propagating acoustic waves produce a standing wave in density, which acts in addition to the stationary temperature component of the grating caused by planes of warmer and cooler molecules.

In order to investigate the dynamics of the grating, a probe beam may be directed into the interference region such that it is incident on the grating at the Bragg angle. The scattered component of the probe beam reflects the dynamics of the thermal grating; the way in which the detected signal varies in time corresponds to the temporal variation of the magnitude of the density modulation of the grating itself.

From the analysis of this signal it is possible to obtain a wealth of information relating to the gas in the measurement region.

1.3 A review of the literature and alternative techniques

The experiments conducted during this study concern measurements in the gas-phase, however laser-induced gratings have also been employed within condensed matter studies to probe the diagnostics of systems in liquid and solid phases, a discussion of which is presented in the textbook of Eichler, Günter and Pohl [6].

In regions of high intensity within a constant volume, when energy from the pump beams is absorbed, the temperature will rise and the density will decrease. In the event of rapid heat deposition, an acoustic wave is formed which propagates outwards. The production of acoustic waves in absorbing media resulting from the interference of two laser beams was described in the 1970's [7]. The production of laser-induced gratings due to quenching as a result of collisions has been well documented [8, 9, 10]. Analysis of the dynamics of thermal, laser-induced gratings has shown scattered signals from a probe laser to reflect the density modulation of the grating, such that the signal is proportional to the square of the density modulation [8]. A probe beam scattered from a LIG provides an attractive way in which to assess an environment; beams scattered in this manner have the coherence properties of, and propagate like, a laser beam. They are therefore ideally suited to remote detection, and since most background sources are isotropic in contrast to the laser-like signal beam, it is possible to collect all of the signal whilst rejecting much of the background. For the application to combustion systems and similarly hostile environments, this presents the significant advantage in data collection outside of a region that is otherwise experimentally difficult to access [10].

The variation of LITGS signals with time was first documented in 1994 and has been described by a number of groups. Comprehensive theoretical analyses have been published by Paul *et al* and Cummings [8, 11]. The technique of LITGS has been employed to probe numerous gas-phase parameters and dynamics. A non-intrusive method to obtain velocity measurements in gases has been devised using the technique of scattering from thermal gratings induced by a pumped Nd:YAG laser similar to that used in this work [12]. The detection of hydrocarbons in addition to other trace species relevant to combustion has been achieved using thermal LIGS in the gas phase, at pressures of up to approximately 1 bar [10, 13]. In the context of combustion, the potential of laser-induced thermal gratings for diagnostic use in flames has been reported following experiments conducted at atmospheric pressure using high temperature gases. The signal detected was reported to have a dependance upon fundamental parameters such as the temperature and composition of the system; it was also noted that measurement of the speed of sound, and hence the temperature, should be possible at known compositions [14]. Experiments conducted within the range of 20-40 bar have indicated that LITGS is also a suitable means by which to determine temperature and pressure in relatively high pressure environments [15].

Successful application of the LITGS technique to determine the temperature of a system via measurement of the speed of sound, the method employed during this work, has also been reported following experiments in the gas-phase, over a broad pressure range and with single-shot measurements by Cummings and colleagues [5, 11]. Although derivation of temperature in this manner was achieved within a 0.5% uncertainty, it was noted that this technique is limited by, and relies upon knowledge of, the gas compositions. Accurate determination of temperature is therefore reliant upon the certainty with which the composition is known, which is of direct relevance to the work presented in this thesis. The application of LITGS to

varying concentrations of NO_2 in N_2 at pressures ranging from 1-40 bar and temperatures within the range of 300-400 K has yielded temperature measurements with precision as low as 0.16% and accuracy of 0.42% [16, 17].

The experimental application of both electrostrictive and laser-induced thermal gratings for gas phase measurements has been reviewed by A. Stampanoni-Panariello *et al* [18], which complements the quantitative theory presented in the corresponding review published by the same group [9]. Here, laser-induced thermal gratings are offered as an attractive experimental technique to provide gas-phase diagnostics as well as fundamental research into the quenching processes that are crucial to the underlying physics. The relative simplicity with which LITGS data may be analysed is also noted as a considerable advantage over alternative techniques used for similar applications, such as Coherent anti-Stokes Raman Scattering (CARS), discussed below [13]. LITGS may also be employed to study molecular relaxation [19]. Such studies have been carried out at temperatures ranging from 300-800 K and pressures between 1-20 bar using mid-infrared radiation, studying NH_3 and C_2H_4 as the absorbing species. Also investigated was the intensity of laser-induced gratings produced using mid-infrared beams in flames, highlighting the feasibility of conducting measurements of this type in such combustion-relevant environments [19].

In the present work, measurements have been made using LITGS applied to gaseous species chosen to include the main contributors to exhaust gas residuals (EGR), air and fuel, in order to quantify the compositional uncertainties in pre-ignition air-fuel mixtures. In previous work, similar methods have also been applied to the detection of minority species present in such an environment. Weak concentrations of NO_2 were detected in ambient air using a laser-induced, thermal grating signal [5]. Investigation of NO_2 in varying air and CO_2 compositions has been carried out using a very similar experimental set-up to that employed during this work

[20]. LITGS signals detected as a result of a beam incident on a grating produced by two overlapping beams, within a sealed cell, yielded measurements of the speed of sound with approximately 1% accuracy for pressures exceeding 1 atm. As mentioned previously, NO_2 has also been used as an absorbing species within N_2 [16]. Using laser-induced grating spectroscopy employing laser beams frequency-matched to resonant transitions within a species, a number of other minor species have also been selectively probed. Using resonant four-wave mixing, a technique in which all four beams involved (the two pump beams, the probe beam and the signal beam) are tuned to one frequency matching that of a known resonant transition within the chosen species, many species have been detected, for example NO [21]. Measurements were recorded at pressures ranging from approximately 0.07-0.1 bar, lower than the pressures used in the work presented in this thesis. Using LITGS, OH has been detected in flames at both atmospheric pressure [14] and higher pressures of 10-40 bar [15]. Laser-induced thermal grating techniques have also been employed to detect H_2O in the gas phase at pressures of 0.02-4 bar, a similar pressure range to that employed in this work, and at both ambient temperatures and in flames [22, 23].

Combustion environments are inherently hostile and many of the experimental efforts discussed above have been conducted under somewhat idealised laboratory conditions. The applicability of laser-induced grating techniques to the study of combustion has, however, been verified by experiments undertaken in combustion-relevant circumstances. The ability to create laser induced gratings within environments containing soot has been demonstrated by Brown and Roberts [24]. Simultaneous determination of parameters including temperature, pressure and concentration has also been achieved using LITGS in a supersonic wind tunnel, employing NO_2 as the absorbing species [25].

The laser-induced gratings that have formed the focus of this discussion are reliant upon resonant absorption of the incident energy supplied to the system by the pump laser beams. The production of gratings via interactions without dependence upon resonance is also possible, however, via the non-resonant process of electrostriction. This is a phenomenon whereby, when subjected to electric fields, materials experience a perturbation in density. In combination with a structured illumination pattern, this process can produce laser-induced gratings and can occur at any incident radiation frequency. With regard to an interference pattern created by two laser pump beams, molecules within the vapour are steered towards regions of higher electric field. This results in a density modulation, and the generation of acoustic standing waves which decay via viscous damping effects within the material [28]. The dominant result of electrostrictive gratings is the production of an acoustic standing wave; stationary temperature modulations such as those produced in the case of thermal gratings play a much smaller part [9, 8, 26]. In the presence of a high concentration of an absorbing species, electrostriction is insignificant in comparison to the thermal effects [5]. The generation of electrostrictive gratings was first presented by Nelson and colleagues, and a theoretical analysis of the way in which electrostrictive gratings are formed has been given by Hubschmid *et al*, [26, 27].

Various mechanisms- both resonant and non-resonant- can result in the production of LIGs within a medium, the theory of which is discussed comprehensively in the review of Stampanoni-Panariello et al [29].

In addition to LITGS, there are a number of other techniques capable of yielding combustion-relevant parameters such as temperature. These techniques can be categorised into two groups; 'linear' and 'non-linear' methods, and a comprehensive overview is given in the review of Kiefer and Ewart [30].

One of the main linear methods of temperature measurement is absorption spec-

troscopy. By tuning a laser or using a dispersive instrument with a broadband illumination source, an absorption spectrum may be measured and the temperature derived from the line shape. The width at FWHM of a Doppler-broadened spectral line is proportional to $\sqrt{T/m}$ where T is the temperature and m is the molecular mass of the species concerned [31].

Another linear method based upon the absorption of photons is Laser-Induced Fluorescence (LIF), which relies upon fluorescent dyes excited by laser beams. Following a molecular transition from the ground to an excited state induced by the absorption of a photon, a spontaneous re-emission of one or more photons occurs at a wavelength longer than (or equal to) the absorbed photon. This may be detected in the form of a multi-line LIF spectrum on a spectrometer. Relative line strengths then provide temperature information, as the populations of the upper and lower states are affected by the Boltzmann distribution and thermalisation effects. Alternatively, dependence of the integrated fluorescence intensity upon temperature may also allow temperature measurements [30, 32]. In terms of applicability to combustion environments, the use of LIF for the derivation of parameters such as temperature has the significant disadvantage that it commonly relies upon the measurement of intensity. Such measurements can vary over time, as components age and optics may slowly go out of alignment. Practically, relying upon intensity measurements in combustion environments can be challenging due to the tendency of combustion products to deposit upon windows used for optical access, which can affect the detected signal intensity.

Within the category of linear methods, Rayleigh scattering may also be employed in order to infer temperature. If the Rayleigh scattering cross-section is assumed to be constant, I_R, the Rayleigh signal intensity, approximates to the number concentration of the species concerned. Assuming constant pressure within a combustion environment, the ideal gas law yields the result that the Rayleigh signal is inversely

proportional to the temperature. The nature and applications of Rayleigh scattering has been reviewed by Zhao and Hiroyasu [34].

Considering non-linear optical methods of temperature determination, perhaps the greatest rival of LITGS is Coherent anti-Stokes Raman Scattering (CARS), a four-wave mixing (FWM) technique reliant upon *stimulated* photon emission resulting from a laser-driven molecular transition. *Spontaneous* Raman scattering involves a transfer of energy between a molecule and incident photon, and is thus described as an inelastic scattering process[1]. The transfer of energy may be either from the photons to the molecule, or vice versa. For the case in which energy is transferred *from* the incident photons *to* the molecule, the emitted photon is of longer wavelength and hence a lower energy. The photon is 'Stokes shifted'. Similarly, when the transfer of energy is from the molecule to the photon, the emitted photon is of a higher energy and may be described as 'anti-Stokes shifted'.

This process is induced during CARS by causing an interaction between three different laser beams, two of frequency ω_1 and one of frequency ω_2. The combination of these beams results in the CARS signal of frequency ω_3, as shown in figure (1.2). Of the two different CARS methods, rotational CARS yields more accurate measurements at temperatures less than 1000 K whilst vibrational CARS is optimal at temperatures exceeding 1000 K, due to the energy spacing of vibrational levels being larger than that of rotational levels [35].

CARS, like LITGS, is a spectroscopic method capable of recovering information regarding parameters that influence combustion efficiency. In comparison to LITGS, however, a CARS experiment is more complex to set up and the procedure of data analysis is significantly more challenging. Using CARS, temperature may be determined via accurate modelling of spectra, although since the method relies

[1]Conversely to Raman scattering, Rayleigh scattering involves no transfer of energy between a molecule and an incident photon, and is therefore described as an elastic scattering process.

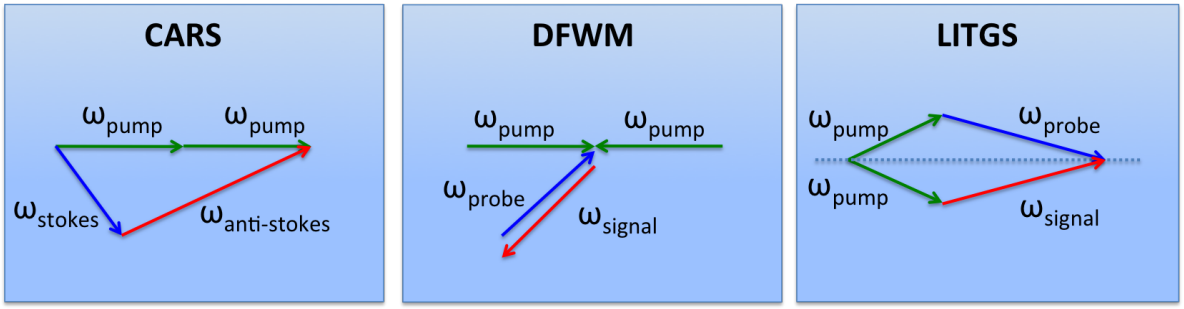

(a) *The beam geometry for LITGS, CARS and DFWM.*

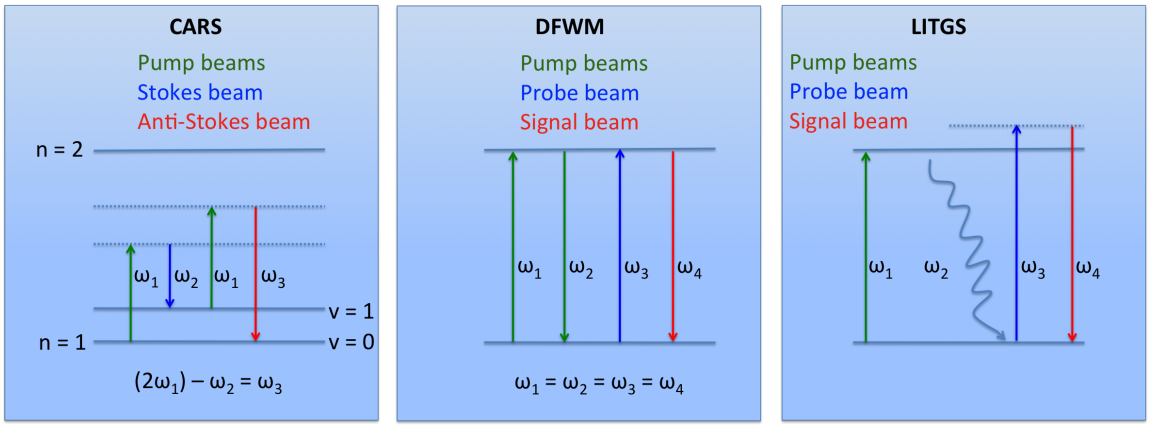

(b) *The molecular transitions in non-linear optical techniques.*

Figure 1.2: The processes of LITGS, CARS and DFWM [36].

on measurement of spectral intensity, the precision of fitting to a modelled spectra is affected significantly by spectral intensity fluctuations. Using LITGS, temperature may be determined using information, namely the oscillation frequency, that is not affected by intensity fluctuations in this manner. Other advantages of LITGS include pump and probe laser beams of different wavelengths which contributes to a high signal to noise ratio.

Other important considerations are the accuracy and precision of the techniques. Measurements of temperature derived from LITGS signals have been shown to have greater precision than analogous measurements obtained using CARS, where single-shot temperature measurements with precision as good as 10% have been reported, at a thermocouple temperature of 300 K [35]. Using a modeless pump laser, a

precision of around 1.6% has been obtained [37]. As discussed above, the use of LITGS to measure temperature can result in precision as low as 0.16% and accuracy of 0.42%, an improvement of approximately one order of magnitude [16, 17].

Chapter 2

LITGS Thermometry

In this chapter, the LITGS technique is described in detail. Initially addressed is the way in which the gratings are produced, and their nature. The method of derivation of the temperature from LITGS signals is presented in section (2.2). Finally, in section (2.3), the appearance of the signals including the reasoning for their decay and oscillatory nature is discussed.

2.1 LITGS

The individual steps that constitute the LITGS process are shown in figure (2.1). Initially, a pump laser beam is split into two and the two beams are crossed within an absorbing gas, such as fuel vapour, creating an interference pattern. Within the regions of high intensity of the fringe pattern, incident radiation is absorbed from the pump beams by the molecules within the vapour, promoting these molecules to an excited state. There are various processes by which it is possible for the excited molecules to decay back to their ground state. These can be grouped into two classes; radiative and non-radiative, according to whether a photon characterised by $\Delta E =$

hc/λ[1] is created during the process of relaxation. Non-radiative de-excitation is known as quenching, and is usually dominant at the kinds of elevated temperatures and pressures typical of the work reported here.

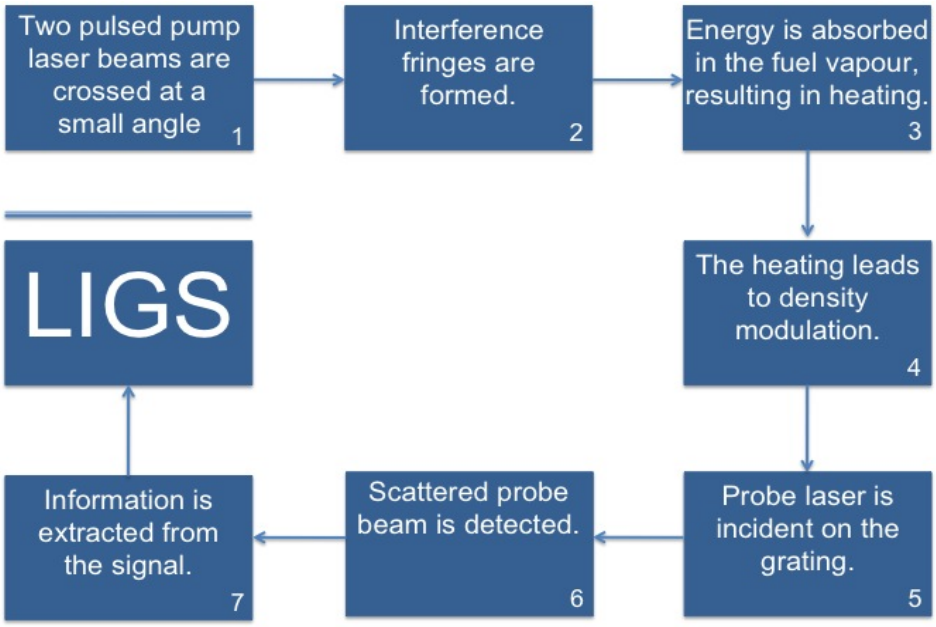

Figure 2.1: *A flow-chart illustrating the LIGS process.*

The quenching process, among others, is illustrated in figure (2.2) [38]. As the molecule decays down the ladder of rotational and vibrational states, due to collisions with other molecules its energy is redistributed in the form of translational kinetic energy (bulk gas heating). The bold lines in figure (2.2) [38] represent electronic states; the lighter lines correspond to the vibrational and rotational sub-levels within the molecule. S_0 indicates the ground state- the lowest energy configuration, and S_1 the first singlet[2] excited state to which an electron is promoted upon absorption of

[1] ΔE is the difference in energy between initial and final molecular states, h is Planck's constant and λ is the vacuum wavelength of the emitted photon.

[2] The term 'singlet' refers to the configuration of electron spins within the system. A singlet has spin angular momentum, s = 0; the direction of the spins of two electrons are opposite (spin-paired). Alternatively, a triplet state has s = 1, with the two electrons having parallel (unpaired) spins.

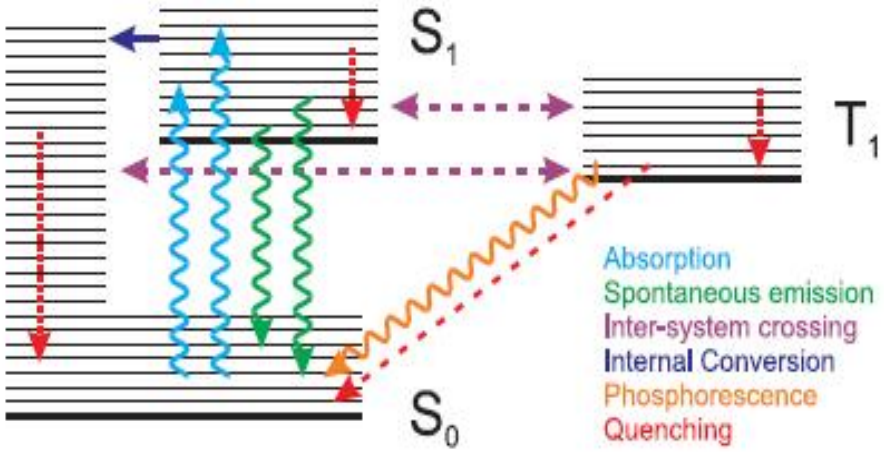

Figure 2.2: *An illustration of energy transfer mechanisms in a molecule. Spontaneous emission refers to the process of fluorescence. The wavy lines represent the absorption or emission of photons. The dashed lines represent the redistribution of ro-vibrational energy [38].*

a photon.

Quenching is crucial to the LITGS technique since the internal relaxation mechanism controls the strength of the thermal grating; weaker quenching results in a weaker thermal deposition.

In order to investigate the dynamics of the system, a continuous wave (cw) probe beam may be directed onto the grating. A majority of the probe beam is transmitted through the grating; it is the scattered component that is of interest. This is detected using, for example, a photodiode or a photomultiplier tube (PMT) as shown in figure (2.3) [38]. The directionality of the beam scattered from the grating is the result of the spatial periodicity of the fringe planes, in a manner similar to the case of x-ray diffraction from crystals; the signal beam is scattered from the grating at an angle matched to the wavelength of the light, given by equation (2.1), the Bragg equation,

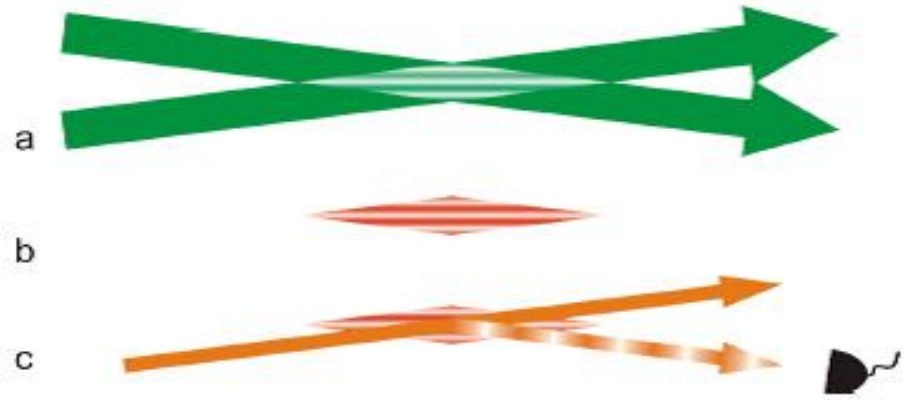

Figure 2.3: *The three phases of generation of a LITGS signal. a) The production of an interference pattern using two intersecting pump beams; b) The red colour represents the production of heat via quenching, which leads to the production of a density modulation feature; c) The (orange) probe beam is incident on the grating, and the scattered component detected as the LIGS signal.*

$$\lambda = 2\Lambda sin\theta, \tag{2.1}$$

where λ is the probe wavelength, Λ is the spacing of the grating planes and θ is the required angle of incidence of the probe beam such that it may be scattered from the grating. The scattered beam is the LITGS signal, a typical example of which is given by figure (2.4).

The time required for an acoustic wave to traverse a fringe spacing is described by τ,

$$\tau = \frac{\Lambda}{c_s}, \tag{2.2}$$

where c_s is the speed of sound and Λ is the spacing between the fringes, given by

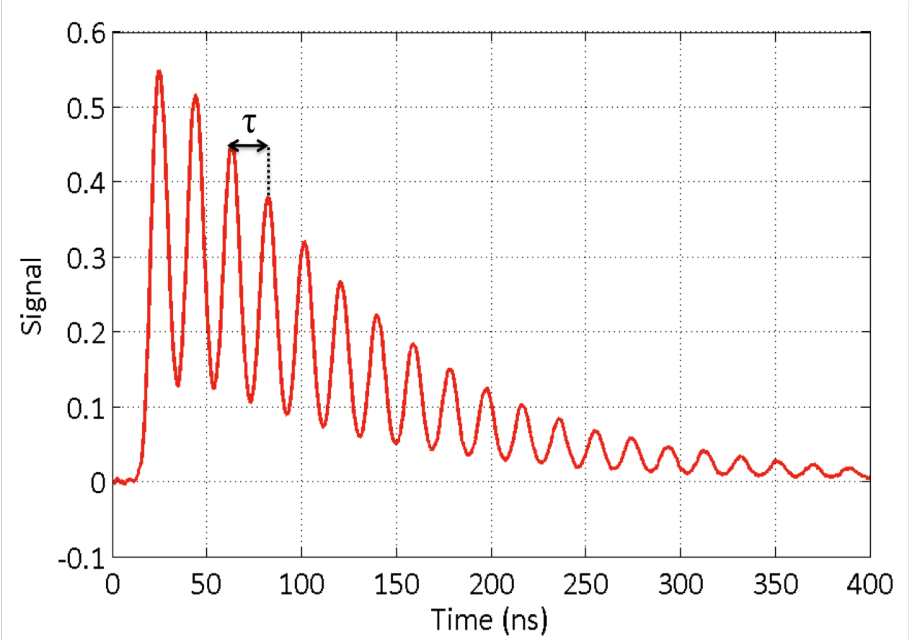

Figure 2.4: *An example of a typical LITGS signal trace obtained within synthetic air (O_2 and N_2) at a total pressure of 4 bar, using acetone as the absorbing tracer species.*

$$\Lambda = \frac{\lambda_{pump}}{2sin(\frac{\theta_x}{2})}, \tag{2.3}$$

where λ_{pump} is the wavelength of the pump laser and θ_x is the angle between the crossed pump beams, as shown in figure 2.5(a).

2.2 Temperature determination

Given the fringe spacing, equation (2.2) enables the determination of the speed of sound; the speed at which the acoustic waves travel within the interaction region. The temperature may then be derived from kinetic theory;

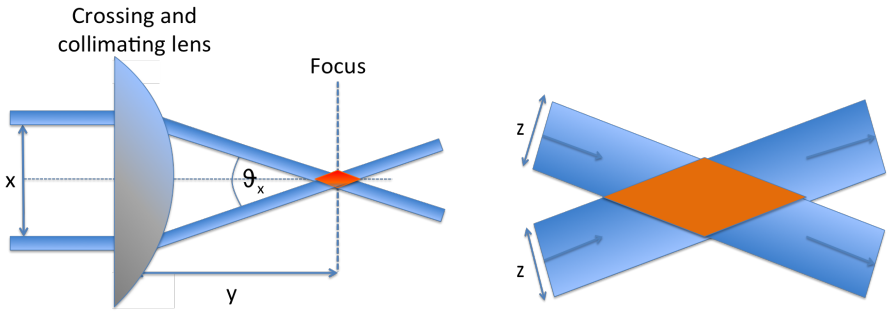

(a) The geometry resulting in the crossing angle, θ_x, of the two pump beams. The separation of the pump beams is denoted by x and y is the focal length of the lens.

(b) The geometry leading to the area of the grating/ interaction (orange) region. The diameter of the pump beams is given by z.

Figure 2.5: *The geometry of the pair of crossed pump beams.*

$$c_s = \sqrt{\frac{\gamma k_B T}{m}}, \tag{2.4}$$

where γ is the ratio of specific heats (C_p/C_v) for the gas present in the interaction volume, k_B is the Boltzmann constant, m represents the molecular mass of the gas and T is the temperature. Substitution of equation 2.2 into equation 2.4 and rearranging for T gives a relationship between T and τ;

$$T = \frac{\Lambda^2}{\tau^2}\frac{m}{k_B\gamma}, \tag{2.5}$$

which may be reduced to;

$$T \propto \frac{m}{\gamma} \tag{2.6}$$

Equation (2.6) is significant because it shows that the parameters γ and m must be known in order that temperature may be derived in this manner. Thus, for accurate derivation of the temperature, a fore-knowledge of the gas composition within the probe volume is necessary. The focus of this study is to quantify the effect of uncertainty in composition on measurement accuracy.

2.3 LITGS signal appearance

The shape of a typical LITGS signal is displayed in figure (2.4). A measure of the absorber concentration may be derived from integration of the signal, and measurement of pressure is possible by measuring the decay rate of the signal [38]. The temperature of the probe volume may be derived using the time period, τ, the reciprocal of the oscillation frequency which may be recovered directly from the LITGS experimental data as shown in figure (2.4). This is the time required for an acoustic wave to travel across a fringe spacing, given by equation (2.2).

In general, LITGS signals begin with a sharp increase in intensity induced by the rapid deposition of energy. There are two characteristic features of a LITGS signal; an oscillation and an exponential decay with time. The latter has two contributions; viscous damping causes the acoustic waves to decay, and diffusion allows the temperature modulation to dissipate until the medium is once again at equilibrium [5]. The oscillatory nature of the signal is the result of the interaction of the travelling acoustic (pressure) waves with the stationary density modulation resulting from changes in temperature. As the acoustic waves traverse the grating, the scattering efficiency of the grating changes, resulting in a modulated signal beam that reflects the dynamics of the grating as a combination of the stationary temperature grating and the travelling acoustic waves.

Chapter 3

Experimental Work

In this chapter, the details of the experiments undertaken will be described. Firstly the apparatus and the experimental set-up will be described. Secondly, the practical method used to obtain LITGS signals is then explained. The methods of data analysis are then presented together with the derivation of the relevant parameters. Finally, experimental difficulties and practical considerations including modifications to the originally intended experimental set-up and limitations of the system are discussed.

3.1 Apparatus and Instrumentation

A Spectron Laser Systems flashlamp-pumped Nd:YAG laser of fundamental wavelength 1064 nm is employed as the pump laser, providing about 30 mJ at the second harmonic, 532 nm. The pump laser beam is frequency quadrupled to 266 nm in order to resonantly excite acetone molecules, used as the absorbing species within a stainless steel pressure cell.

The green light produced by the pump laser is vertically polarised. The con-

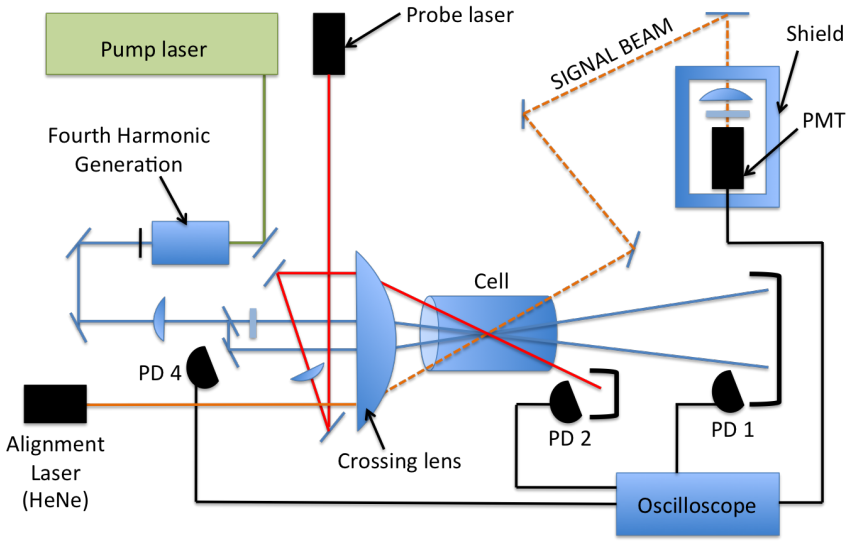

Figure 3.1: *LITGS experimental apparatus. Shown in the diagram is the apparatus allowing the intersection of two Nd:YAG pump beams within the cell. A HeNe laser beam (the red line) is aligned to follow the path of the probe and signal beam in order to align the signal beam onto the detector (PMT). The grating is probed using a Diode-Pumped Solid State Laser (DPSSL).*

version efficiency of the KD*P crystal from green to UV is approximately 3.5%, producing horizontally polarised UV light of 1.1 mJ per pulse. The residual green light exiting the crystal is vertically polarised. The polariser shown in figure (3.2) passes only horizontally polarised light; the green is rejected into a beam dump. The strength of the UV signal is monitored prior to grating production by photo-diode PD 4, shown in figure (3.1). This can be optimised by adjusting the angle of the frequency doubling crystal in order to maximise the intensity of the UV pump beams, and hence the LITGS signal.

The pump beam is split into two using a 50% reflecting plate beamsplitter, and one beam is passed through a fused silica optical compensator in order to make an adjustment for the optical delay induced between the two beams by the splitting process; it is important to ensure that when both beams arrive at the crossing region, they do so within a coherence length of each other. The coherence length can be

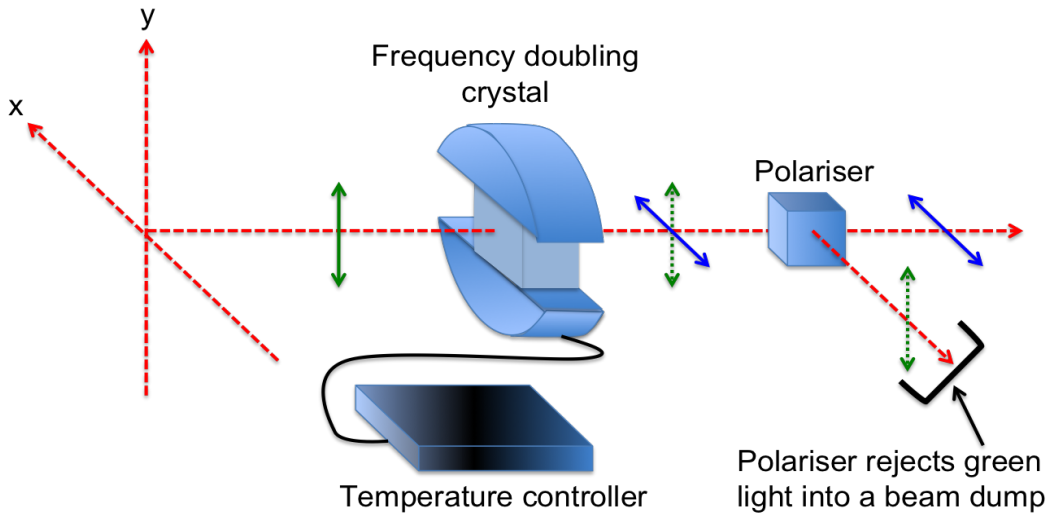

Figure 3.2: *The system used to double the frequency of the green light emitted from the pump laser to produce UV light. Horizontal polarisation is illustrated in the x-direction, vertical polarisation in the y-direction. The green arrows indicate the polarisation of green light at each stage of the process; the blue arrows illustrate the polarisation of the UV light.*

approximated to the inverse of the linewidth; the typical linewidth for a multimode Nd:YAG laser is 1 cm^{-1} [39]. This is important because if the two beams do not oscillate within a fixed phase relationship, their interaction would not produce a spatially constant fringe pattern; in this case, the fringe pattern would blur, and a LITGS signal would not be generated.

Following the splitting of the pump beam, both beams are passed through a collimating and crossing lens of 50 mm diameter and focal length 235 mm at 266 nm, which crosses the beams at the focal point of the lens according to the geometry illustrated in figure (3.3). Prior to the pump beam being split, it is passed though an f = 50 cm plano-convex fused silica lens which forms a telescope with the crossing lens. The interaction region is enclosed within a cylindrical stainless steel cell of diameter ∼4 cm and length 30 cm fitted at either end with fused-silica windows of thickness 12.7 mm and diameter 50 mm, providing optical access to the cell interior.

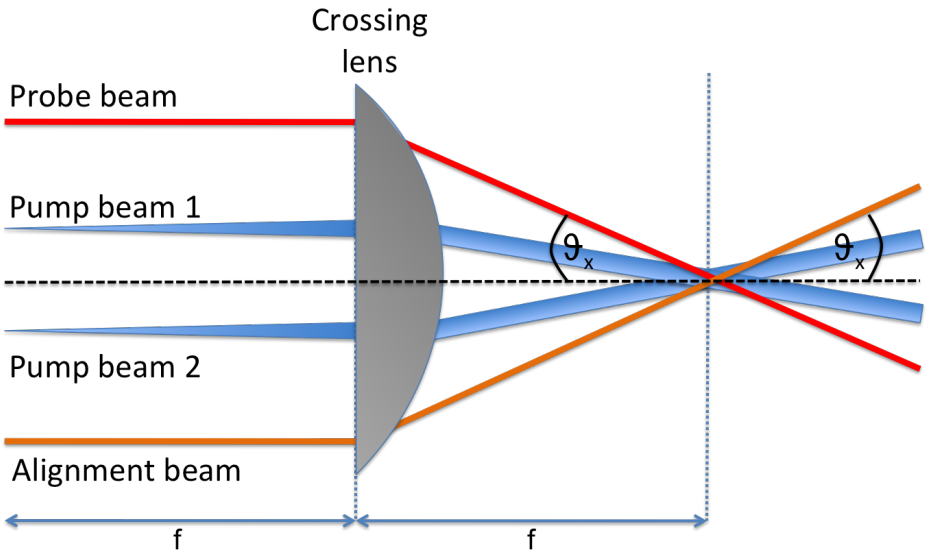

Figure 3.3: *The geometry of the crossing region. The alignment beam used is generated by a HeNe laser, which simulates the path of the signal beam.*

Liquids are administered via syringe into the cell via a valve. Following production of the thermal grating, the pump beams are directed into beam dumps and photodiode PD 2 is used to detect the intensity of the pump beams.

The grating is probed using a 300 mW continuous wave (cw) diode-pumped solid state laser that emits a beam of wavelength 671 nm, aligned such that it is incident at the Bragg angle with respect to the grating planes. The direction of the beam scattered from the grating is traced by a helium neon (HeNe) laser beam. The signal is detected using a Hamamatsu H6780-20 photomultiplier tube (PMT) as shown in figure (3.1). The intensity of the component of the probe beam that does not contribute to the LITGS signal and is transmitted through the grating is monitored using photodiode PD 3, shown in figure (3.1). Prior to detection, the signal beam passes through a RG610 (red glass) filter in order to prevent interference between the LITGS signal and stray light of wavelengths shorter than 610 nm. Both the filter and the PMT are optically shielded using black cardboard, as shown in figure (3.4).

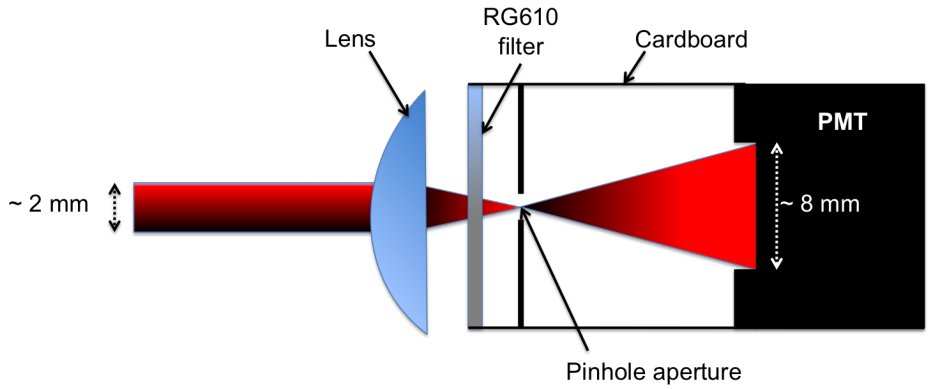

Figure 3.4: *The system used to detect the LITGS signal. A plano-convex lens is used to focus the signal beam such that it diverges to fill the PMT window in order to avoid saturation of the photocathode; the beam is passed through a 'longpass' filter and a pinhole aperture in order to reject any scattered light.*

The intensities of the LITGS signal, the incident and transmitted pump beams and the probe beam are recorded by a LeCroy 'waverunner' 6050A oscilloscope, and extracted using an external USB drive such that they may be analysed on a PC.

3.1.1 Alignment procedure

A system consisting of two masks is used through which the pump, probe and HeNe alignment beams are aligned. One mask is positioned before the interaction region and one afterwards, both containing holes through which the beams are directed. Firstly, the two pump beams are considered as shown in figure (3.5), starting with the upper beam which is aligned using mirrors 1 and 2. The lower beam, split using the reflecting plate beamsplitter labelled 3 in figure (3.5), is aligned using beamsplitter 3, which adjusts the position of the beam and mirror 4, which adjusts its angle.

When successfully aligned through both masks, the pump beams run parallel to each other as indicated in figure (3.6(a)). The crossing lens is then installed, which collimates and crosses the beams within the region that is to be enclosed by the cell.

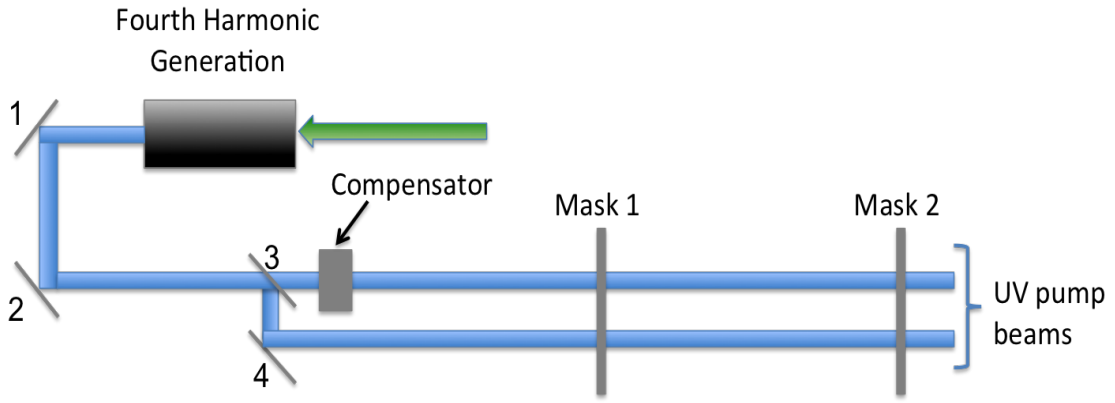

Figure 3.5: *During the initial stage of alignment, a duo of masks is used through which the pump beams are directed prior to the introduction of the crossing lens.*

Minor adjustments may be made using the screws on the crossing lens in order to perfect the alignment of the pump beams onto mask 2.

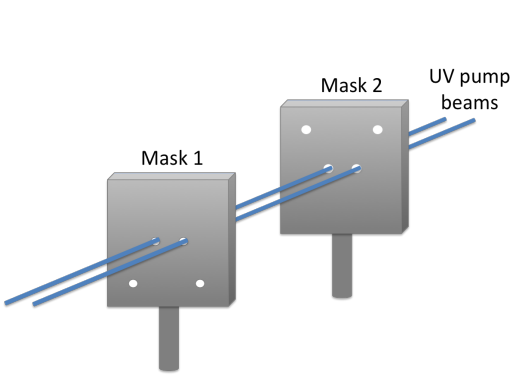

(a) The alignment of the pump beams through both masks, such that they run parallel to each other prior to the introduction of the crossing lens.

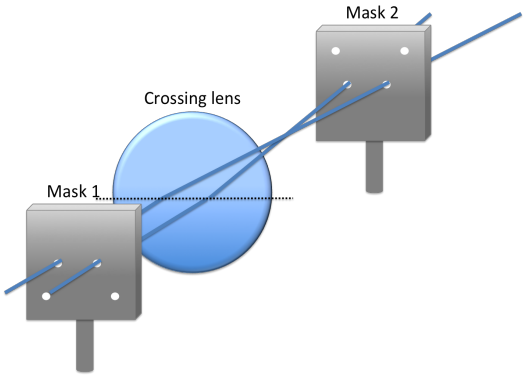

(b) The beams are crossed, defining the interaction region.

Figure 3.6: *The alignment of the pump beams.*

Figure (3.7) illustrates the process of creating crossed and collimated pump beams in order to produce the desired interaction volume, the crossing lens shown

as lens *b*.

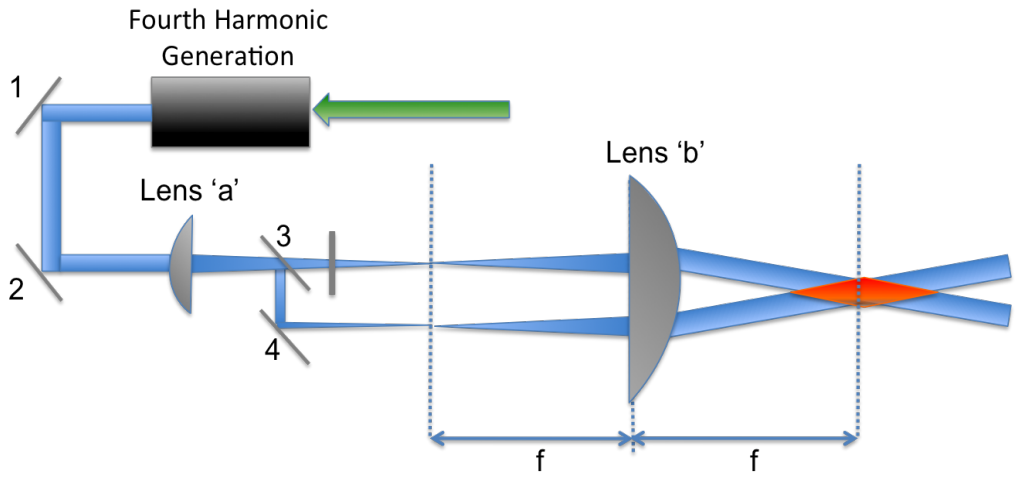

Figure 3.7: *The introduction of the crossing lens, lens b and lens a, which ensures that the beams are collimated when they cross.*

Upon introduction of the crossing lens, lens *a* is installed also, its purpose being to ensure that the pump beams are diverging when they reach the crossing lens such that they may be collimated. In the absence of lens *a*, the beams would be collimated when they reach the crossing lens, which would then focus both beams such that the interaction volume would be reduced. This would result in fewer grating planes being produced, which would artificially limit the duration of the LITGS signal.

A pinhole of approximately 100 μm diameter is placed at the crossing point prior to the introduction of lens *a*, through which the HeNe beam is aligned to follow the path of the signal beam, through mask 2 and onto the detector. The probe beam is then aligned through the pinhole onto mask 2. This procedure, shown in figure (3.8), ensures that the probe beam is incident precisely at the location of the grating, and requires delicate adjustment; the pinhole is positioned at the exact crossing location using a translation stage.

The pinhole and mask 2 are then both removed, and the three mirrors between

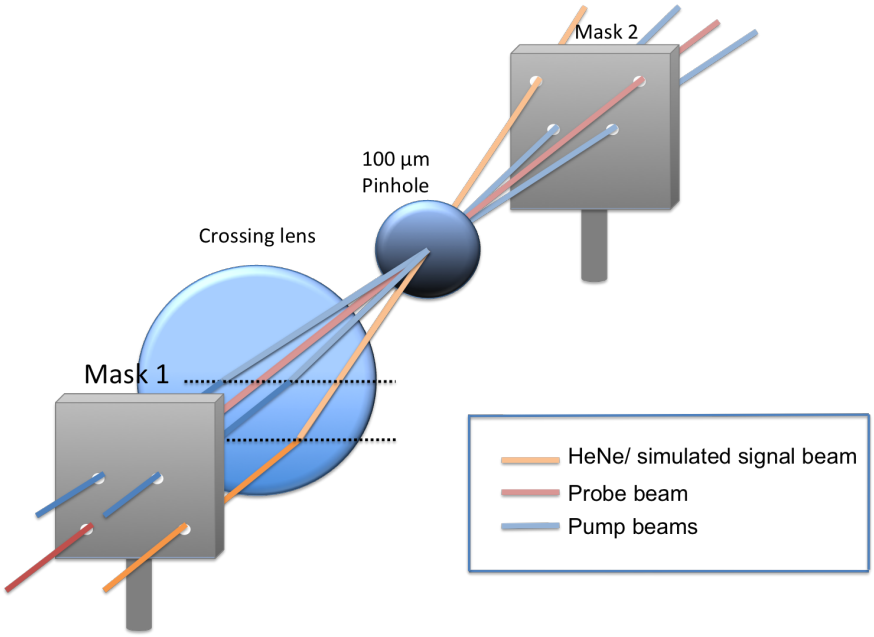

Figure 3.8: *The alignment of the HeNe (simulated signal) beam and the component of the probe beam not diffracted from the grating through the crossing location and onto mask 2.*

the cell location and the PMT shown in figure (3.1) are used to optimise the alignment of the simulated signal beam onto the PMT.

Prior to installation of the cell, the pinhole is replaced by a piece of plastic tubing containing absorbing vapour (either toluene or acetone) that is centred around the crossing location. This is used to optimise the strength of the LITGS signal and to confirm that the alignment procedure has been successful. The tube containing vapour is then removed, and the cell installed.

3.1.2 Temperature measurement

Since the oscillation frequency of LITGS measurements is temperature dependent, it is crucial that the variation in cell temperature is kept to a minimum during LITGS data collection; a Eurotherm temperature controller is used to maintain both the cell and the vapour contained within it at constant temperature. A PT100 resistance

thermometer, used as a temperature sensor, is secured to the outer surface of the cell wall as shown in figure (3.9) and is soldered to two wires leading to a proportional band temperature controller. A length of electrothermal NiChrome wire is wrapped around the outer body of the cell in uniformly spaced coils, covering the entire length of the cell. Both ends of the NiChrome wire are connected to wires leading to the temperature controller output.

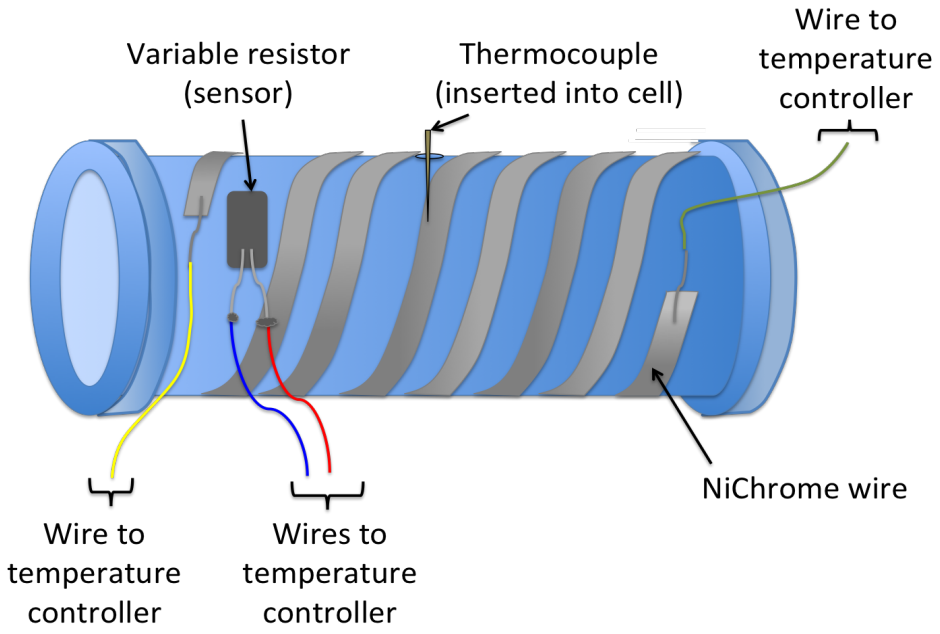

Figure 3.9: *Temperature control arrangements for the LITGS test cell.*

The temperature controller may be set to a maximum temperature of 99.9°C[1].

A thermocouple, inserted into the cell as shown in figure (3.9), is used to measure the temperature of the gas within the cell. This is positioned above the crossing region, however not directly in it so as not to interfere with the paths of the pump

[1]The cell temperature is raised by the heater current and detected by the sensor, which exploits the change in resistance incurred by a small electrical current supplied to it; the PT100 has a resistance of 100 Ω at 0°C. As the cell temperature increases, the resistance of the PT100 does likewise; this change is relayed to the temperature controller in order to raise the current supplied to the NiChrome wire until the temperature controller registers a resistance from the PT100 that corresponds to the desired temperature.

and probe beams.

3.1.3 Pressure measurement

The cell is connected to a manifold constructed using 6.35 mm stainless steel piping, allowing access to the gas cylinders used during LITGS experiments. Each cylinder is connected to the manifold via a valve and a regulator. The pressure of gases admitted to the cell is measured using a Drück PDCR810 pressure transducer, which records pressure in bar gauge[2]. All experiments were conducted at a total pressure of 4 bar; an example of the experimental schedule sheet completed during LITGS experiments, which records the pressures admitted to the cell in order to produce gas mixtures of certain compositions, is included in Appendix A.

3.2 Data analysis

Data analysis has been conducted using the MATLAB numerical computing environment, produced by MathWorks, Inc. The method used to extract the oscillation frequencies of LITGS signals from the raw data builds upon MATLAB code written previously by Dr. Ben Williams, with the addition of modifications by the author which are indicated at the top of each code. All MATLAB codes are displayed in Appendix B.

There are three main functions written in MATLAB that contribute to the analysis of the raw data recorded on the oscilloscope, all three of which are brought together and "called" by a fourth piece of code. The first of these functions, entitled ReadFiles_v3_f.m, is used to convert the raw data into a format convenient for analysis; a MATLAB file. This takes the form of a five-column array consisting of both time and the raw data gathered from oscilloscope channels 1-4 which represent

[2]i.e. relative to atmospheric pressure.

the input pump intensity, the output pump intensity, the probe intensity and the signal, as shown in figure (3.10).

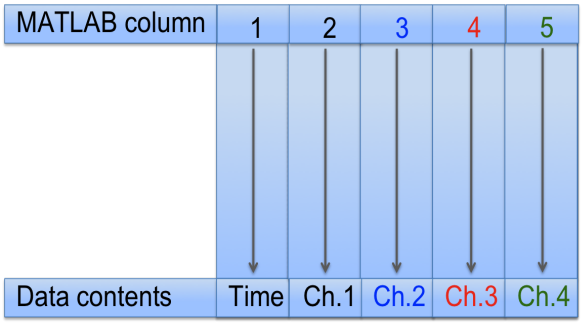

(a) The contents of the MATLAB data files following conversion from the raw data.

Oscilloscope channel	Data contents
Ch.1	Pump (output)
Ch.2	Pump (input)
Ch.3	Signal
Ch.4	Probe

(b) The recorded data corresponding to each channel on the oscilloscope.

Figure 3.10: Conversion of the raw data to a MATLAB file.

The four channels on the oscilloscope produce signal traces as shown in figure (3.11).

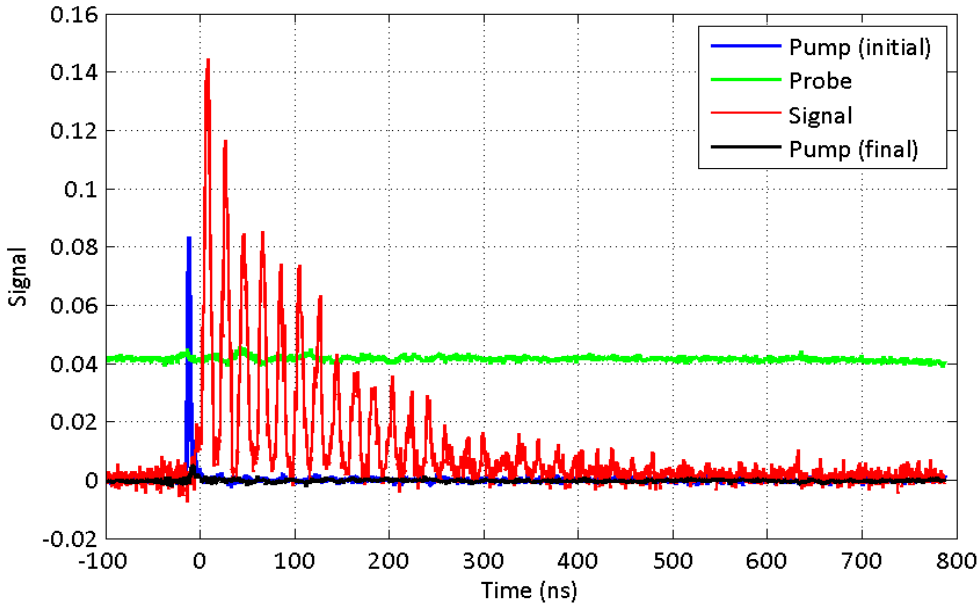

Figure 3.11: *The appearance of the signal traces recorded by all four detectors included in the experimental apparatus.*

The second function employed during the data analysis procedure is MakeIA_v2_f.m, the purpose of which is to sequentially cycle through the data traces recorded by the oscilloscope in order to discard any signals low enough to be dominated by noise and any high enough to have saturated. The function operates by firstly loading the MATLAB data file created from the raw data by ReadFiles_v3_f.m. The noise value is evaluated by calculating the standard deviation of the first 5 % of samples during a shot and multiplying by ten. Any signals with a maximum value falling below three times this limit are considered to be noise and rejected.

The upper limit, above which values are discarded in case of saturation of the detector is 600 mV. Saturation of the oscilloscope's analogue to digital converter is avoided by discarding the strongest signal and any that have the same peak value.

Finally, the function saves the data that falls within the chosen limits into an output folder, from which the oscillation frequencies of each LITGS signal may be

calculated.

The mean oscillation frequencies of the LITGS signals and the corresponding values of standard deviation, which are plotted as the error in the oscillation frequency, are calculated by the third function, OscFrq_f.m. Firstly the data set containing all values falling between the designated upper (saturation) and lower (noise) limits is loaded. The fast Fourier transform (FFT) of the time-series data is computed in order to convert to the frequency domain. This enables a power spectrum to be plotted using a code entitled PowerSpectrum.m, and the oscillation frequency at the peak of each LITGS oscillation to be recorded as shown in figure (3.12).

A vector containing the peak frequencies of oscillation as derived from the power spectrum is saved, in addition to the mean of this vector, representing the mean oscillation frequency of each composition tested and the standard deviation, the variation within the frequency vector.

Finally, the three functions described above are called into a code entitled ProcWrapper.m, which iteratively applies each of the functions in turn to each data set considered. Firstly the variables specific to a particular test composition are entered, including the molecular mass, m, and the ratio of specific heats, γ, of each species. The individual tests themselves are then identified using their title; all tests are saved according to their composition in millibar; for example, a test composition consisting of 200 mbar CO_2 and 3800 mbar N_2 is saved as '200-3800'. Once all individual data sets have been analysed by all three functions, a final function entitled fitting_oscfrq.m is called, which produces a plot of mean oscillation frequency, f_{osc}, with respect to γ/m. The ratio of γ/m is calculated according to weighted averages given by equations (3.1) and (3.2).

$$m = m_1 \times \left(\frac{P_T - P_P}{P_T}\right) + m_2 \times \left(\frac{P_P}{P_T}\right), \tag{3.1}$$

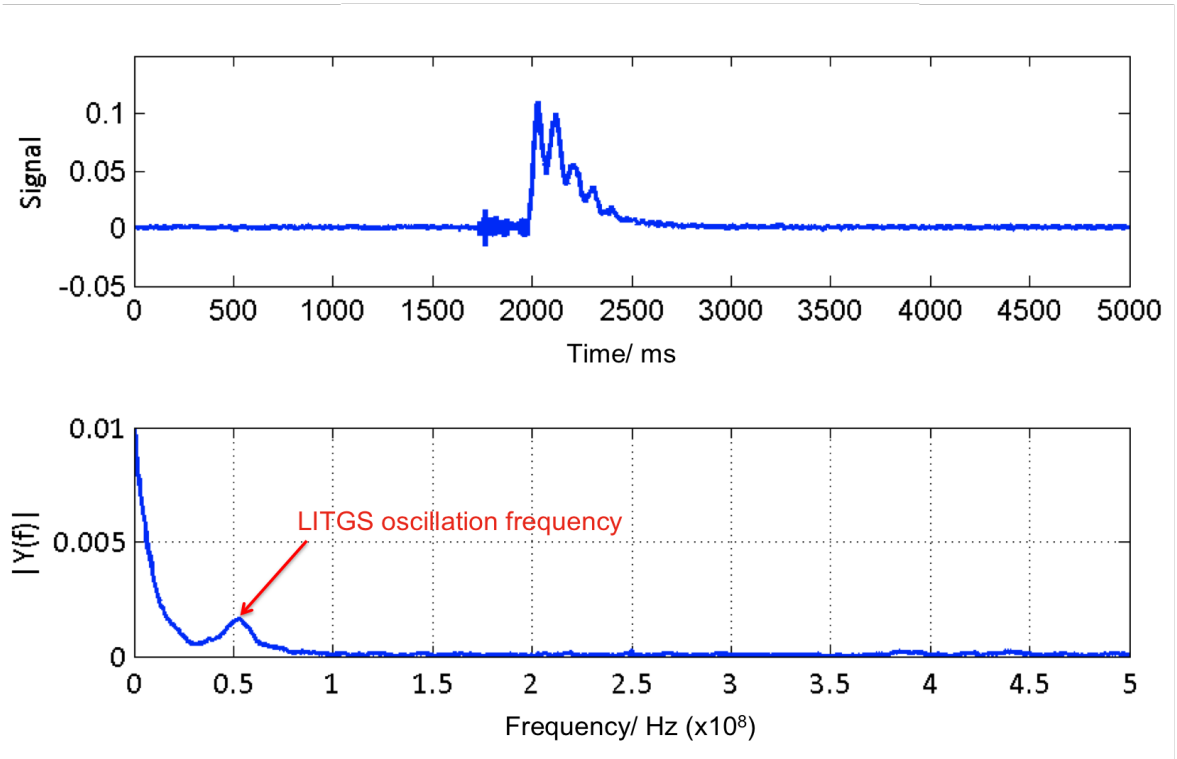

Figure 3.12: *A typical LITGS power spectrum. The modulus of the fast Fourier transform allows the oscillation frequency to be identified. In this case, it is approximately 55 MHz.*

where m_1 is the molecular mass of one species in a two-species compositional mixture, m_2 is the molecular mass of the other species, P_P is the partial pressure of the first species and P_T is the total pressure which, during all LITGS experiments, was kept constant at 4 bar. The ratio of specific heats for a particular composition is calculated similarly;

$$\gamma = g_1 \times \left(\frac{P_T - P_P}{P_T}\right) + g_2 \times \left(\frac{P_P}{P_T}\right), \tag{3.2}$$

where g_1 is the ratio of specific heats of one species and g_2 is the ratio of specific heats of the other. At this stage, a line is also produced using the 'polyfit' command in MATLAB. This will be described in more detail in section (4.3).

3.3 Experimental difficulties and limitations

During the LITGS experiments a number of small difficulties and limitations of the system became apparent, some requiring modifications to the experimental apparatus.

The most notable modification was the introduction of the temperature controller in order to choose and regulate the temperature of the cell, and the vapour contained within it, to temperatures higher than ambient (approximately 25°C). This was a worthwhile addition since preliminary tests revealed that the temperature of the cell rose by approximately 0.4 % during the course of a LITGS experiment. Since the oscillation frequency is dependent upon and sensitive to small fluctuations in temperature, it was necessary to minimise this effect; the temperature controller was used in order to raise the cell temperature above that of its environment in order to avoid a gradual increase in temperature. Thus, all LITGS experiments other than those conducted at deliberately higher temperatures were undertaken at 30°C. Further motivation for the use of the temperature controller was the inability to evaporate, at ambient temperature, the volumes of liquid required to conduct tests including varying volumes of water and fuel.

Despite the success of the temperature controller in maintaining the cell and vapour temperature at constant values sufficient to evaporate the fluid volumes required, final experiments revealed that this method does not heat the cell windows sufficiently. Since the fused-silica cell windows act as less efficient conductors than the stainless steel cell, the temperature of the windows was commonly lower than that of the cell body. This effect did not inhibit tests solely involving gases, however it did result in the condensation of water on the inner surfaces of the windows. In order to keep the required volumes of water in the vapour phase, it was found to be necessary to use a hairdryer to heat the cell windows continuously until all liquid

had returned to the vapour phase. This process, for 2.7 ml of water (the greatest volume tested), took approximately one hour. Thus, a significant improvement to the system would be a method to maintain the temperature of the cell windows at a value comparable to that of the cell walls.

Although sufficient for the experiments conducted during this work, the maximum gas temperature that the temperature controller is capable of maintaining within the cell is 80°C. In order to simulate scenarios that might be expected to occur within combustion environments, significantly higher temperatures would be required. This could be seen to be a limitation of the current experimental apparatus.

Chapter 4

Results

Presented in this chapter are the results obtained from the LITGS experiments conducted in order to investigate the effect of compositional variations on the oscillation frequency of LITGS signals. Firstly, the results obtained using varying gas compositions including CO_2, O_2 and N_2 are investigated, and the effect of a saturated vapour pressure of water discussed. In all experiments, two drops (16 μl) of acetone are used as the absorbing species.

Secondly, a study is presented during which the volume of fuel is systematically varied in a constant total pressure of N_2, in order to assess the effect of fuel alone on the oscillation frequency. A similar study is presented using varying concentrations of water, the aim of this experiment being to determine the effect of varying volumes of H_2O on the oscillation frequency of the signal in a dry EGR mixture.

Finally, a number of tests have been conceived and undertaken in order to simulate various compositions of air, fuel and EGR such as might occur during the compression stroke of an engine, and are also compared to predictions.

The errors associated with the measurement of γ/m for each composition are quoted in the captions underneath the corresponding graphs.

4.1 Determination of errors in γ/m

For the plots showing the variation in oscillation frequency with γ/m, the errors in γ/m were calculated according to the combination of partial pressures of the constituent components of a particular composition that result in a mean value of γ/m furthest from the mean; a 'worst case' scenario.

The factor that most greatly influences the accuracy of γ/m for the tests involving solely gases is the accuracy with which the required partial pressures are admitted to the cell. The variation in the intended value is taken to be $\pm$ 10 mbar.

The greatest source of error in γ/m for the experiments conducted in the presence of a saturated vapour pressure of water within the cell, calculated according to the Antoine equation, is the certainty with which the temperature is known, and maintained at the constant value required. Thus, for the greatest deviation from the mean value of γ/m, a temperature variation of $\pm$ 5°C has been accounted for.

Finally, the greatest contribution to the error in γ/m for the experiments conducted using varying concentrations of fuel and water is the uncertainty in the mass of an individual drop. This was taken to be the standard deviation between the masses of ten drops as measured by a 'JENCONS-PLS HM-120' balance. The results of the analysis of the errors in γ/m for all compositions of gases, water and fuel tested are displayed in table (4.1).

Table 4.1: *The percentage error in* $\gamma/$m.

Test Composition	% Error in γ/m
O_2-N_2	$\pm$ 0.2
O_2-N_2-H_2O	$\pm$ 0.5
CO_2-N_2	$\pm$ 0.4
O_2-N_2-H_2O	$\pm$ 0.2
CO_2-O_2-N_2	$\pm$ 0.2
C_8H_{18}-N_2	$\pm$ 0.1
H_2O-N_2-CO_2	$\pm$ 0.4

4.2 The effect of pressure

It can be seen from figure (4.1(b)) that at a total pressure of 1 bar the signal duration is considerably shorter than that exhibited at 4 bar; this is due to the higher diffusion rates prevalent at lower pressures, resulting in a shorter lifetime of the density modulation. In addition, the depths of the LITGS oscillations at 1 bar are less than those at 4 bar.

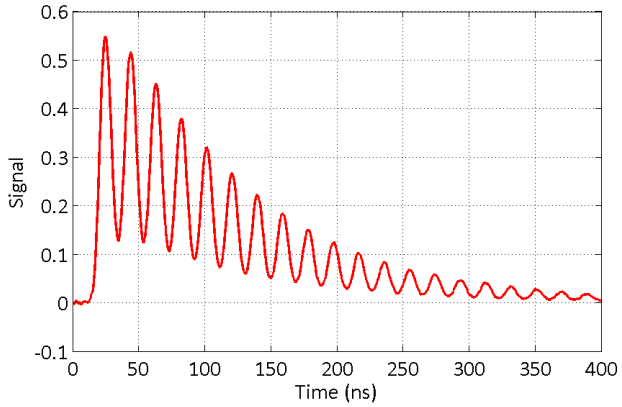

(a) *A LITGS signal (arbitrary units) averaged over 50 shots, obtained from a composition of O_2 and N_2 containing 60% O_2 at a total pressure of 4 bar.*

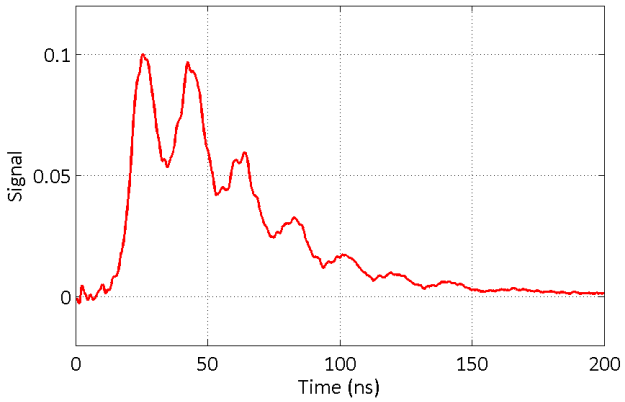

(b) *A LITGS signal (arbitrary units) averaged over 50 shots, obtained from a composition of O_2 and N_2 containing 60% O_2 at a total pressure of 1 bar.*

Figure 4.1: *The effect of pressure on LITGS signals.*

This effect is a result of decreased collisional quenching at lower pressures leading to a reduced thermalisation rate and weaker density modulation in comparison to that at higher pressures.

Practically, this results in LITGS signals at lower pressures comprising fewer oscillations than those at higher pressures. Oscillation frequency may be derived with more precision when there are more peaks in the signal, because this results in a narrower peak in frequency space; all experiments have therefore been conducted at a total pressure of 4 bar.

4.3 Theoretical fit for plots of f_{osc} vs. γ/m.

It should be noted that the theoretical fit displayed as a red line on all plots in this chapter showing the variation in oscillation frequency as a result of changes in γ/m is a 'fit' to the data, rather than the result of a full a theoretical model.

This is calculated according to the fact that the oscillation frequency is proportional to the ratio γ/m, and the variables used for the ratio of specific heats and the molecular mass are those relevant to each individual composition. The mean ratios of γ/m for each composition are calculated according to the MATLAB code entitled 'FittingOscfrq.m' using the variables specific to each species involved.

In addition to the result that the oscillation frequency is proportional to the square root of γ/m, substituting $\tau = 1/f_{osc}$ into equation (2.2) gives;

$$c_s = \Lambda \times f_{osc}, \tag{4.1}$$

where c_s is the speed of sound and Λ is the spacing of the grating planes, and from equation (2.4),

$$f_{osc} \propto \sqrt{\frac{\gamma}{m}} \tag{4.2}$$

the 'polyfit' command in MATLAB is then used to construct a best-fit according to the format given in equation (4.3).

$$f_{osc} = k\sqrt{\frac{\gamma}{m}} + c. \tag{4.3}$$

The fit used is therefore not simply an arbitrarily-chosen polynomial, rather it is motivated by the expected physical relationship, and can be used to indicate the degree to which the data does or does not conform to the underlying trends of the chosen theory.

4.4 Repeatability of LITGS signals

.

The reproducibility of the oscillation frequency of LITGS signals is illustrated by figure (4.2). Figure (4.2(a)) displays the repeatability of the oscillation frequencies determined from two separate data sets resulting from varying concentrations of O_2 in N_2 with water vapour absent from the overall composition. An analogous comparison with the addition of a saturated water vapour within the cell is shown in figure (4.2(b)). Both plots demonstrate good repeatability of measurements of oscillation frequency derived from LITGS signals, suggesting that factors such as minor changes in the alignment do not significantly affect the oscillation frequency.

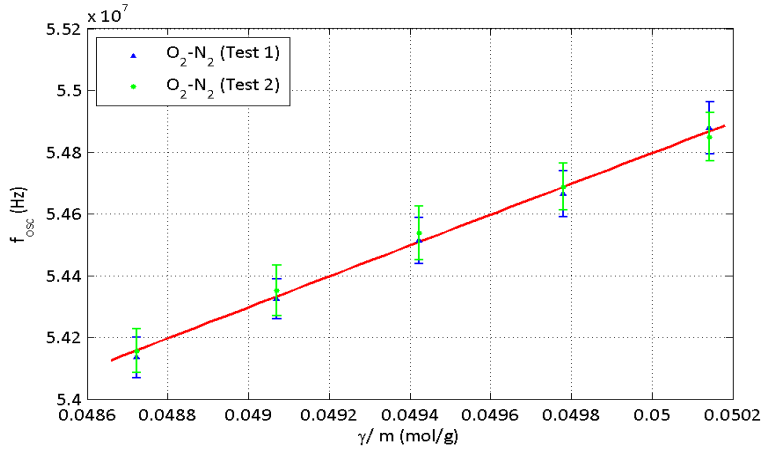

(a) *Reproducibility test without H_2O; varying compositions of O_2 and N_2 at a total pressure of 4 bar were repeated to assess the reproducibility of the measurements of oscillation frequency.*

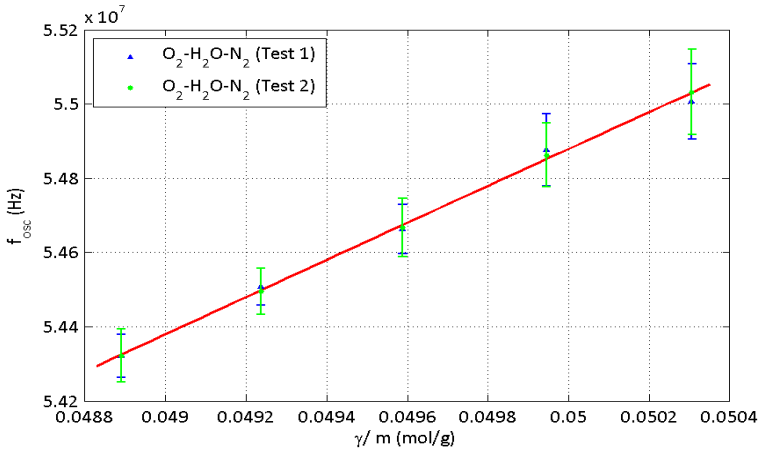

(b) *Reproducibility test with H_2O; varying compositions of O_2 and N_2 at a total pressure of 4 bar, in addition to a saturated water vapour, were repeated to assess the reproducibility of the measurements of oscillation frequency.*

Figure 4.2: *Reproducibility of LITGS measurements.*

4.5 Gas species in combustion

Table (4.2) shows the composition of dry air. When air is mixed with fuel in order to combust the fuel, the ratio of air to fuel must be correct for complete combustion to occur. Equation (4.4) shows how fuel and air react to produce post-combustion gases.

Table 4.2: *The mean mass and γ of air, weighted according to the contribution of the constituent gases, are 28.97 g and 1.406 respectively.*

Gas	% Fraction	Mass (g/mol)	γ	Weighted Mass (g/mol)	Weighted γ
N_2	78	28	1.404	21.84	1.095
O_2	21	32	1.400	6.72	0.294
Ar	1	40	1.670	0.4	0.0167

Assuming the fractional composition of air shown in table (4.2), the percentage of each gas present in a typical post-combustion gas mixture is calculated according to equation (4.4);

$$C_8H_{18} + \alpha\left(\frac{21}{21}O_2 + \frac{78}{21}N_2 + \frac{1}{21}Ar\right) = \beta(CO_2) + \gamma(H_2O) + \delta(N_2) + \epsilon(Ar), \quad (4.4)$$

On the left hand side of equation (4.4) are the reactants; fuel (iso-octane, C_8H_{18}) and air, and on the right hand side the products, referred to as exhaust gas. In an IC engine application, the exhaust gas is often referred to with the acronym EGR, which stands for exhaust gas residuals. The percentage that each of CO_2, H_2O, N_2 and Ar contribute to EGR may be determined by balancing the species on the left and right hand sides of the equation such that, for example, α represents the number

of moles of air and β represents the number of moles of CO_2. It should be noted that the percentages that these values correspond to assume the idealised scenario of complete combustion. In the event of complete combustion, this method indicates that 1.6% fuel would be required for a stoichiometric mixture of air and fuel. To account for the fact that combustion is rarely complete, the fractional contributions of the main species present in EGR have been scaled to accommodate a total of 2 % trace species, including O_2, CO, traces of fuel and oxides of nitrogen. The resulting composition is given in table (4.3), where the relative proportions of the trace gas species is motivated by chapter 2 of *'Introduction to Internal Combustion Engines'* by Professor R. Stone [40].

Table 4.3: *The mean mass and γ of EGR, weighted according to the contribution of the constituent gases, are 28.73 g and 1.38 respectively.*

Gas	% Fraction	Mass	γ	Weighted Mass	Weighted γ
N_2	71	28	1.404	19.88	0.99684
H_2O	14	18	1.33	2.52	0.1862
CO_2	12	44	1.300	5.28	0.156
Ar	1	40	1.670	0.4	0.0167
O_2	1	32	1.400	0.32	0.014
CO	0.5	28	1.400	0.14	0.007
C_8H_{18}	0.1	114	1.08	0.11423	0.00108
NO	0.25	30	1.400	0.075	0.0035

Tables (4.2) and (4.3) show that the main gas species present in air and EGR are O_2, N_2 and CO_2. The results shown in the following sections indicate firstly the effect upon the oscillation frequency when these gases are varied, secondly the combination of gases and water and finally the introduction of fuel.

4.6 Compositional effects: gases

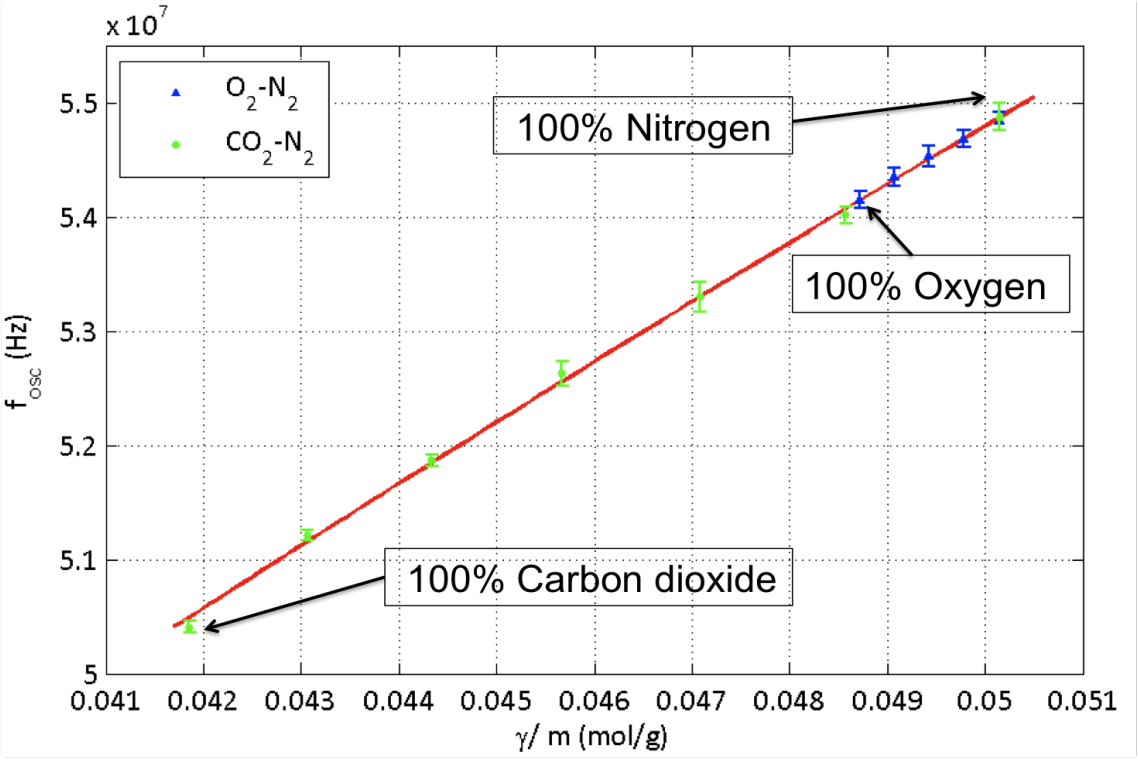

Figure 4.3: *The oscillation frequency measured from LITGS data recorded at varying compositions of O_2 and N_2 (the upper right of the plot) and a total pressure of 4 bar, compared with an analogous experiment conducted using CO_2 and N_2 (increasing CO_2 towards the bottom left of the plot; the bottom left data point consists of 100 % CO_2. The percentage error in γ/m has been calculated to be $\pm$ 0.2 % and $\pm$ 0.4 % for the tests comprising O_2-N_2 and CO_2-N_2 respectively, assuming a likely error in partial pressure of not more than 10 mbar. Further details regarding the calculation of the percentage error in γ/m may be found in section (4.1).*

The effect of varying gas composition on the oscillation frequency in the absence of fuel or water contributions is illustrated by figures (4.3) and (4.4). Figure (4.3) shows the variation in oscillation frequency exhibited by LITGS signals recorded in syn-

thetic air (varying concentrations of O_2 in N_2) and dry, simulated post-combustion gases containing CO_2 and N_2. Since the molecular mass of CO_2, 44 g/mol, is significantly higher than that of both O_2 and N_2, the value of γ/m for CO_2 (0.030) is lower than that for either O_2 (0.044) or N_2 (0.050); as expected, this is illustrated by both figure (4.3) and (4.4). It can also be seen that the oscillation frequency increases with increasing γ/m as predicted by equation (4.2); in each figure, both data sets display good agreement with the theoretical fit.

The effect on the oscillation frequency of the addition of CO_2 to synthetic air is shown by figure (4.4), which exhibits the expected increase in γ/m associated with the addition of CO_2. It can be seen that both sets of experimental data correlate well with the predicted trend, indicated by the line of theoretical fit.

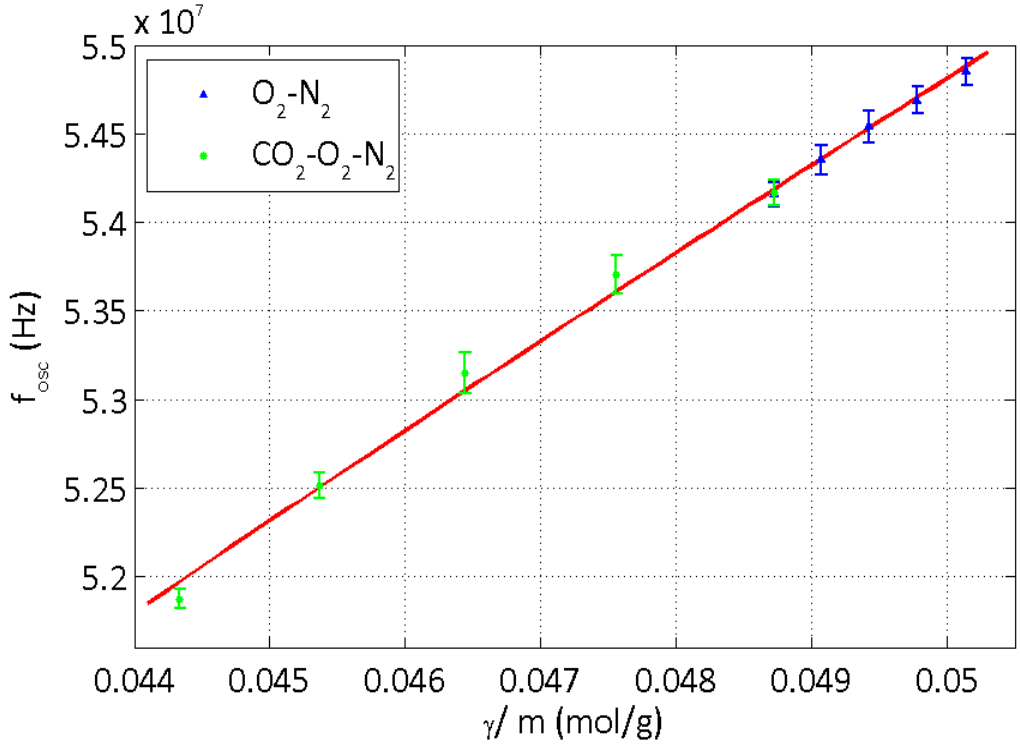

Figure 4.4: *The oscillation frequency measured from LITGS data recorded at varying compositions of O_2 and N_2 at a total pressure of 4 bar, compared with data resulting from a repeat of the same experiment with the addition of CO_2. The percentage error in γ/m has been calculated to be $\pm$ 0.2 % for the tests comprising both O_2-N_2 and CO_2-O_2-N_2.*

4.7 Compositional effects: gases and water

As shown in table (4.3), water constitutes 14 % of EGR. The saturated vapour pressure of H_2O can be calculated according to the Antoine equation [41],

$$\log_{10} P = A - \frac{B}{(C+T)}, \tag{4.5}$$

where P is the vapour pressure (bar), T is the temperature (K) and A, B and

C are the Antoine coefficients for the species considered. The Antoine coefficients used for water and iso-octane, the fuel used in subsequent experiments, are given in table (4.4) [41].

Table 4.4: *The Antoine coefficients. At a temperature of 30° C, these yield pressures of 4.28 kPa for H_2O and 8.32 kPa for C_8H_{18}, as calculated using the Antoine equation.*

Species	A	B	C
H_2O	4.65430	1435.264	-64.848
C_8H_{18}	3.93679	1257.840	-52.415

Figure (4.5) shows the effect of a saturated water vapour on varying compositions of synthetic air at 30°C and 4 bar. Measurements of the oscillation frequency of LITGS signals recorded in concentrations of O_2 in N_2 were repeated with the sole exception of the presence of a saturated water vapour. It can be seen from each pair of data points that γ/m corresponding to the 'wet' measurements is systematically increased with respect to the 'dry' measurements due to the addition of water. The oscillation frequency is increased in the presence of water, and a number of data points suggest that it may be just possible to resolve the presence of water. The ultimate conclusion, however, is that this quantity of water vapour has only a negligible effect on the oscillation frequency of the thermal grating signal.

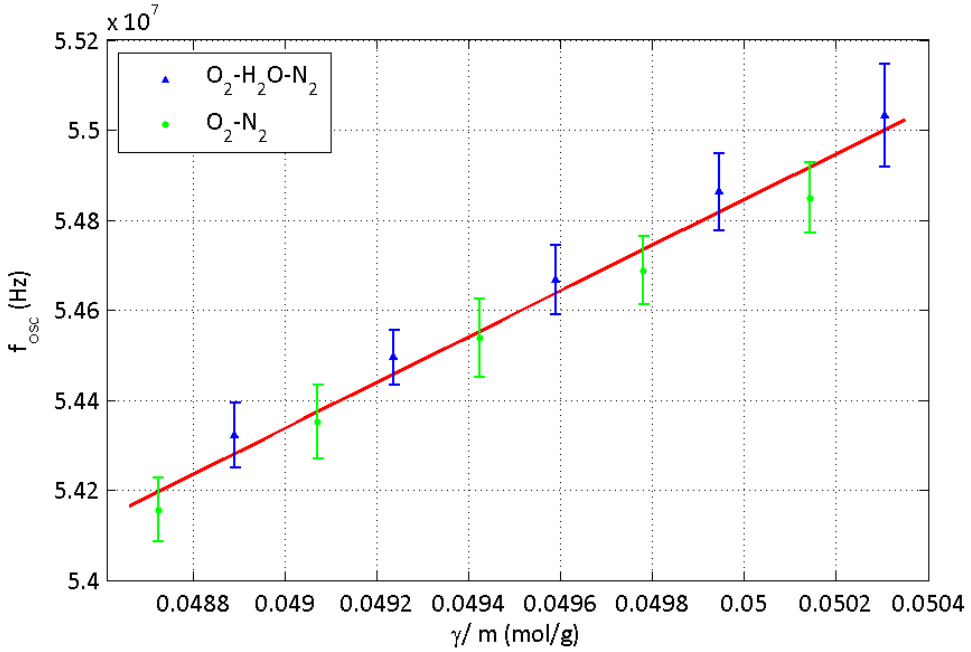

Figure 4.5: *The oscillation frequency measured at varying compositions of O_2 and N_2 at a total pressure of 4 bar, with and without a saturated vapour of H_2O present within the cell. The triangular blue point to the right of each circular green point represents the oscillation frequency of the LITGS signal at the same composition, with the addition of H_2O. Each data point is averaged over 50 shots, the error bars representing the standard deviation within them. The percentage error in γ/m has been calculated to be $\pm$ 0.2 % and $\pm$ 0.5 % for the tests comprising O_2-N_2 and O_2-H_2O-N_2 respectively.*

A similar experiment was conducted using varying concentrations of CO_2 in N_2; figure (4.6) illustrates a comparison between analogous data recorded in the presence of dry and wet synthetic EGR, respectively. Similarly to the case in which synthetic air was considered, figure (4.6) suggests that the effect of water in EGR on the oscillation frequency is small. The addition of a saturated water vapour to these mixtures of CO_2 and N_2 also appears to not cause any problems for the theory, since all data points continue to lie on the best fit line.

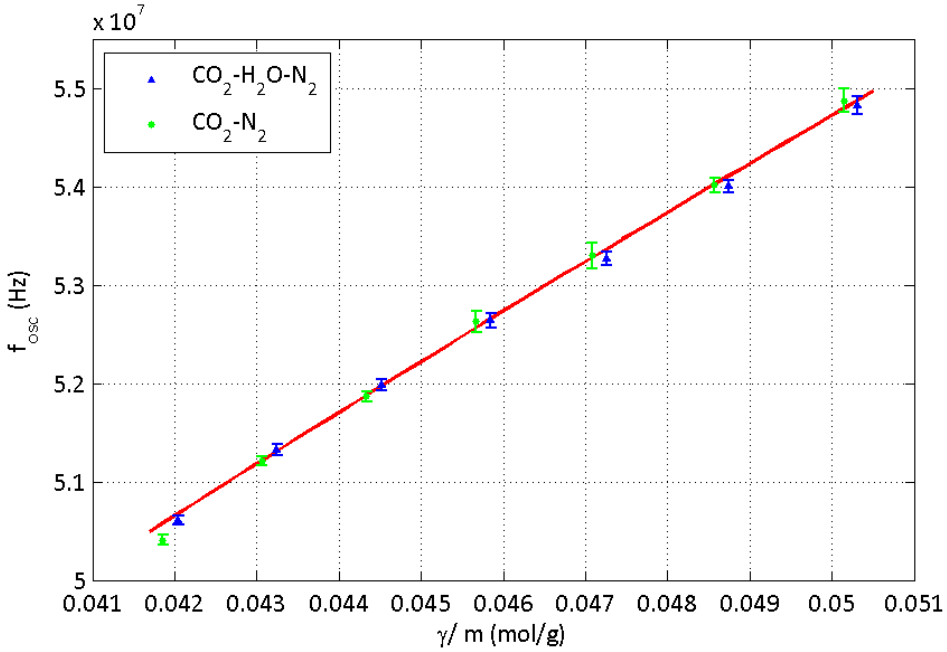

Figure 4.6: *The oscillation frequencies measured at varying compositions of CO_2 and N_2 at a temperature of 30° C and a total pressure of 4 bar, with and without a saturated vapour of H_2O present within the cell. The triangular blue point to the right of each circular green point represents the oscillation frequency of the LITGS signal at the same composition, with the addition of H_2O. Each data point is averaged over 50 shots, the error bars representing the standard deviation within them. The percentage error in γ/m has been calculated to be $\pm$ 0.4 % and $\pm$ 0.2 % for the tests comprising CO_2-N_2 and CO_2-H_2O-N_2 respectively.*

The effect of temperature on the oscillation frequency of LITGS signals is illustrated by figure (4.7). This displays the results of an analogous experiment to that shown in figure (4.6), with the exception that the data set, recorded without a saturated water vapour within the cell, was undertaken at a temperature of 25°C; 5°C lower than that recorded in the presence of a saturated water vapour.

The effect of the difference in temperature between the two experiments is clear to see; the oscillation frequencies of the compositions tested at 30°C are shifted

upward by approximately 4 MHz owing to an increased speed of sound, c_s, at higher temperatures.

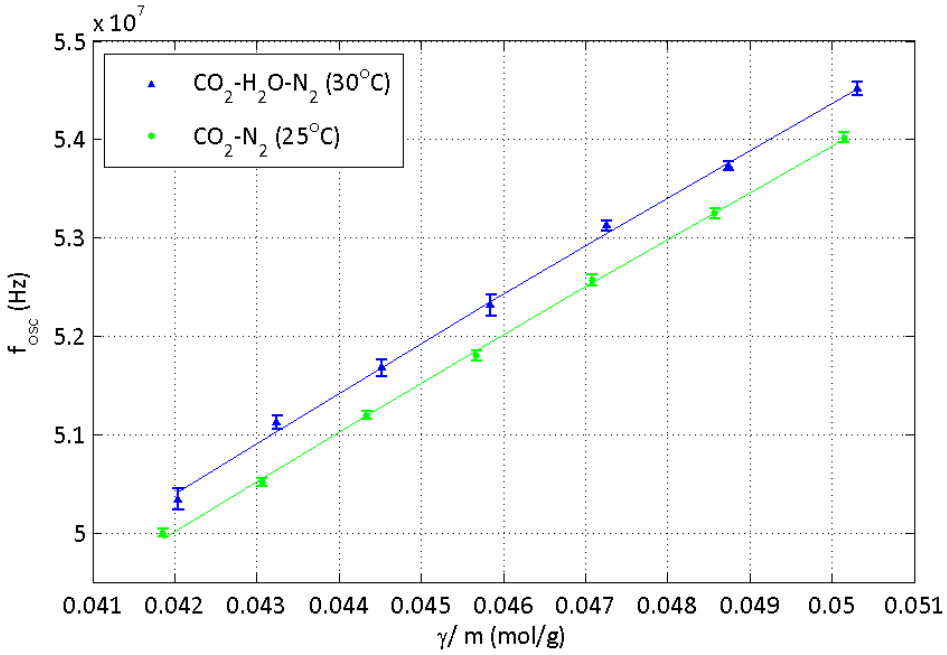

Figure 4.7: *The oscillation frequency measured at varying compositions of CO_2 and N_2 at a total pressure of 4 bar, with and without a saturated vapour of H_2O present within the cell. The two experiments were conducted with a temperature difference of 5°C between them. The percentage error in γ/m has been calculated to be ± 0.4 % and ± 0.2 % for the tests comprising CO_2-N_2 and CO_2-H_2O-N_2 respectively.*

4.8 Compositional effects: water

Although the results presented in section (4.7) correlate well with the theoretical prediction, a saturated water vapour pressure of 4.28 kPa in a total pressure of 400 kPa is far too small to replicate a combustion environment given the target of 14 %. More realistic compositions have been achieved by raising the cell temperature to accommodate a higher water vapour content, and measuring the oscillation fre-

quency of LITGS signals in the presence of varying concentrations of water vapour, admitted to the cell via syringe. Figure (4.8) illustrates the effect of increasing H_2O concentrations in synthetic EGR at a temperature of 80°C, the highest achievable using the temperature controller.

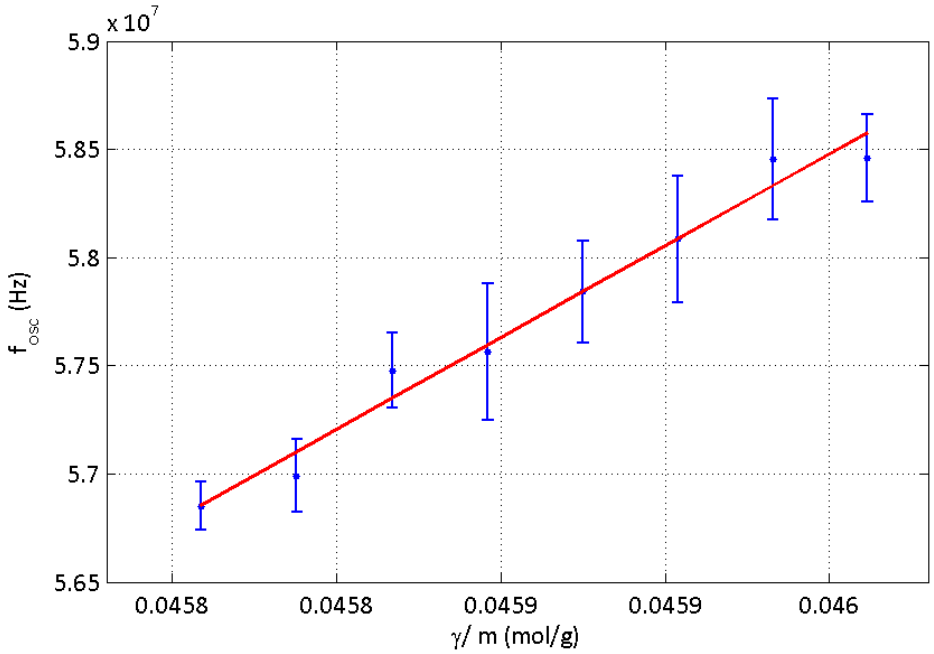

Figure 4.8: *The effect of increasing quantities of H_2O in dry EGR gas on the oscillation frequency. Measurements were recorded at a total pressure of 4 bar and temperature of 80 °C. The percentage error in γ/m has been calculated to be ± 0.4 %.*

It can be seen that for varying concentrations of water the theoretical fit correlates well with the experimental results. Note also that the values on the y-axis have increased relative to previous figures, as a result of the increased cell temperature which was required to retain this quantity of water in the vapour phase.

4.9 Compositional effects: fuel

In order to indicate the effect of fuel alone on the oscillation frequency, varying concentrations of iso-octane (2,2,4-trimethyl-pentane, C_8H_{18}) were admitted to the cell with a 4 bar total pressure of N_2. As can be seen from figure (4.9), the impact of fuel on the oscillation frequency of LITGS signals still does not induce deviation from the theoretical fit. This is an encouraging result, which demonstrates that the theory appears to capture all of the physical information required to characterise the change in oscillation frequency.

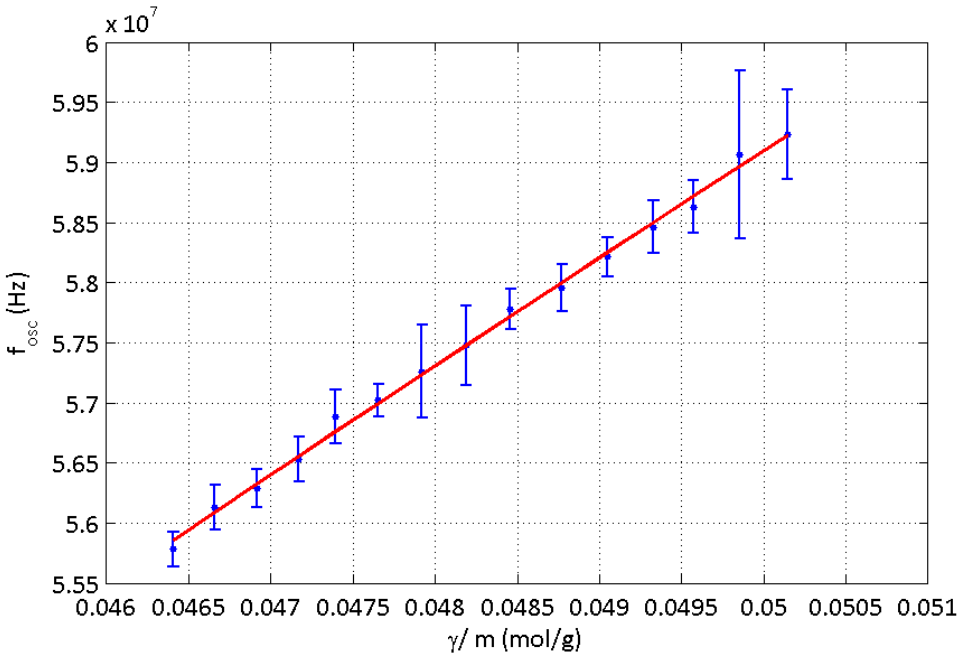

Figure 4.9: *The effect of increasing volumes of C_8H_{18} in N_2 on the oscillation frequency. Measurements were recorded at a total pressure of 4 bar and temperature of 80 °C. The percentage error in γ/m has been calculated to be ± 0.1 %.*

4.10 Simulated engine compositions

Following the excellent agreement between the trends of the experimental data and the theory, a comparison will now be made under conditions where more species are mixed together at a time. Within an engine cycle, different regions may contain varying mixtures of EGR, air and fuel. A system of tests has been designed in order to simulate certain compositional situations that may occur during the pre-ignition compression stroke of an engine cycle, and are summarised in the table below.

Table 4.5: *Tests chosen to simulate different possible compositional situations within pre-ignition gas and fuel mixtures in an engine.*

Test	Simulated Engine Situation	% Fuel	% Air	% EGR
1	A pocket of gas containing pure EGR.	0	0	100
2	A location containing no fuel or EGR.	0	100	0
3	A stoichiometric air-fuel mixture.	1.6	98.4	0
4	An approximately realistic pre-ignition composition.	1.4	83.4	15
5	A location with excess fuel; a rich mixture.	5.1	79.9	15
6	A fuel-deficient location; a lean mixture.	0.4	84.6	15
7	A region with a 50:50 air:EGR composition.	0	50	50
8	A region containing a non-stoichiometric mixture.	2.5	47.5	50
9	A region with an unusually high EGR content.	1.6	18.4	80

The above tests have been conducted using dry EGR (constituting CO_2 and N_2). The omission of H_2O is due to the experimental difficulty in retaining the concentrations required in the vapour phase. Thus, these tests represent an indication of the way in which the oscillation frequency would be affected by such compositional variations; a modified experimental set-up would be required in order to repeat the

tests with the required volume of water to make 'real' EGR.

For each test, the partial pressures of each species contributing to the overall composition have been calculated for simple EGR containing 12 % CO_2 and 71 % N_2, and synthetic air containing 79 % N_2 and 21 % O_2. Also calculated were the partial pressures of H_2O and C_8H_{18} vapour and the corresponding volume of each species in the liquid phase. Since liquids are metered into the cell using a syringe, in order to introduce the correct volume of liquid into the cell the volume can be converted to a 'number of drops', noting the volume of one drop from the syringe used:

Table 4.6: *The masses of a drop of water, iso-octane and acetone measured using a 'JENCONS-PLS HM-120' balance. The error stated is the standard deviation in the measurements of the masses of ten individual drops of each species.*

Species	Mass per drop (kg)
H_2O	$3.28 \times 10^{-5} \pm 1.3$
C_8H_{18}	$1.1 \times 10^{-5} \pm 0.6$
C_3H_6O	$1.26 \times 10^{-5} \pm 0.4$

$$P_{liquid} = N_d \times \left(\frac{M_d \times 1000}{m}\right) \times \left(\frac{R \times T_{cell}}{V_{cell}}\right), \tag{4.6}$$

where P_{liquid} is the partial pressure of the H_2O or C_8H_{18} vapour within the cell, N_d is the number of drops of liquid corresponding to the required concentration, M_d is the mass, in grams, of one drop, m represents the molecular mass of the liquid in g/mol, R is the ideal gas constant, T_{cell} is the cell temperature measured in Kelvin and V_{cell} is the volume of the cell in m^3.

The temperatures required to evaporate the required number of drops for each

of the nine tests are shown in figures (4.10) and (4.11).

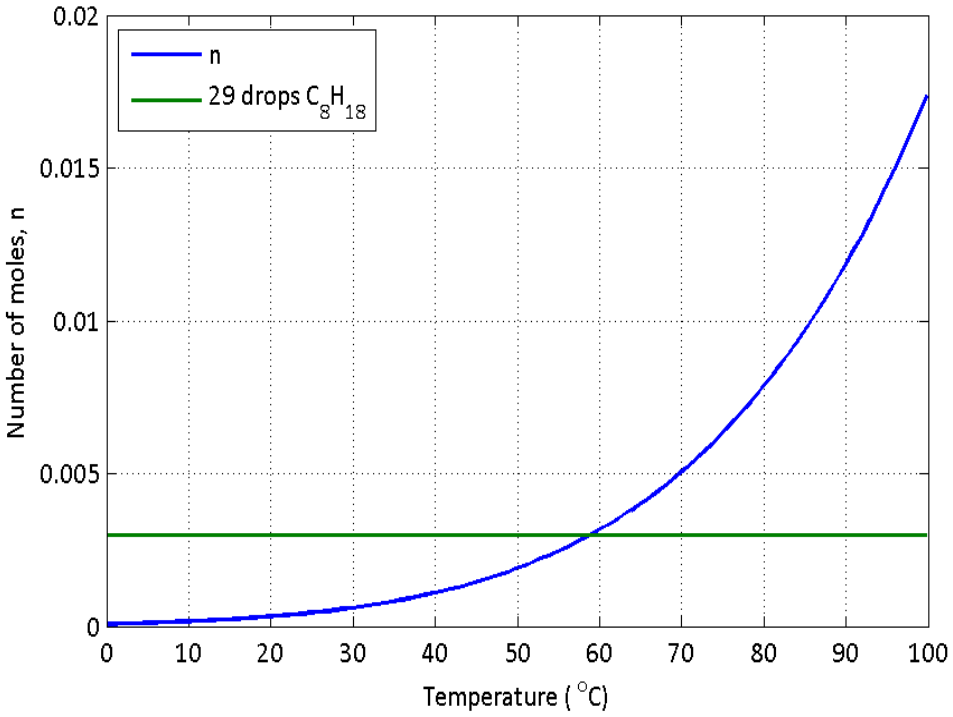

Figure 4.10: *The evaporation characteristics of C_8H_{18}. The horizontal (green) line represents the number of moles in 29 drops of C_8H_{18}, the quantity corresponding to the greatest concentration of fuel required for any of the nine tests specified (test number 5). The blue curve indicates the number of moles of C_8H_{18} that would completely evaporate at a given temperature. The point at which the two lines cross indicates the temperature required to evaporate 29 drops of C_8H_{18}.*

The curve representing the number of moles of each species that can fully evaporate at a given temperature has been calculated by equating the Antoine equation, given by equation (4.5), and the ideal gas law,

$$PV = nRT, \tag{4.7}$$

where P is pressure (Pa), V is volume (m^3), T is temperature (K) and n represents the number of moles. Rearranging both the Antoine equation and the ideal gas law in terms of pressure and equating gives;

$$n = \frac{V}{RT} \times 10^{[A - \frac{B}{(C+T)}]}, \tag{4.8}$$

where n is the number of moles that will evaporate at a given temperature, T.

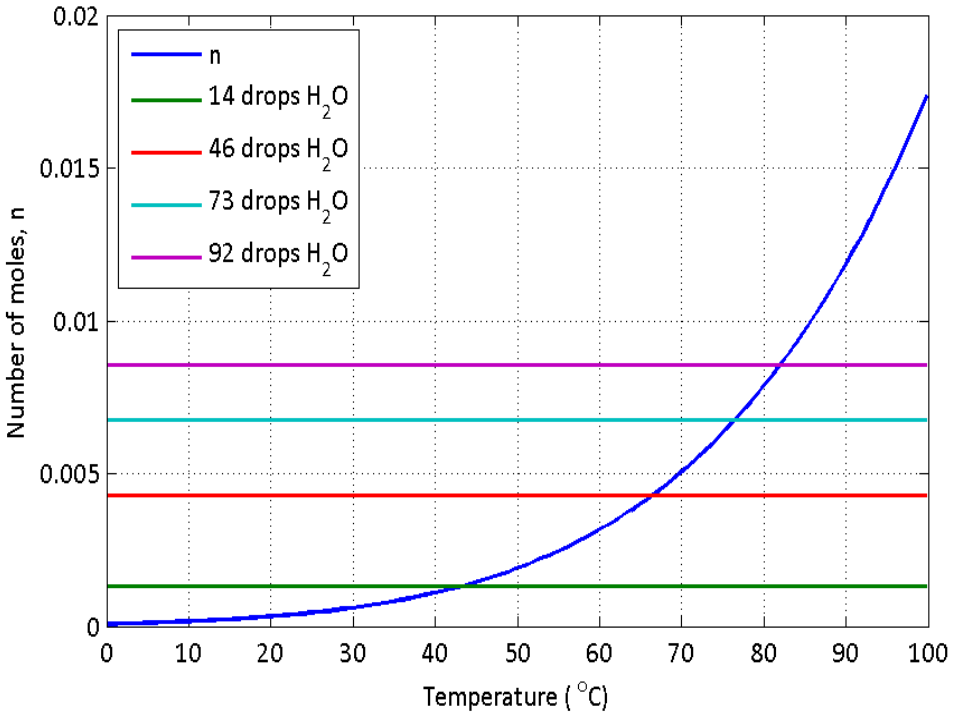

Figure 4.11: *The evaporation characteristics of H_2O. The blue curve indicates the number of moles of H_2O that would completely evaporate at a given temperature. The intersections of this line with the horizontal lines, each representing a different volume of H_2O required for the correct percentage of EGR in each test composition, indicate the temperatures required to keep each volume in the gas phase.*

It was found that although the temperature required to evaporate the greatest

volume of water is approximately 82°C, only just above the maximum regulated gas temperature, experimentally it was not possible to achieve this because water condensed on the inner surface of the windows. As a result of this, the tests have been undertaken using 'dry' EGR.

Figure (4.12) illustrates the composition of the nine tests described in table (4.5), where each test number is located at the intersection of the coordinates that correspond to the percentages of EGR and fuel present.

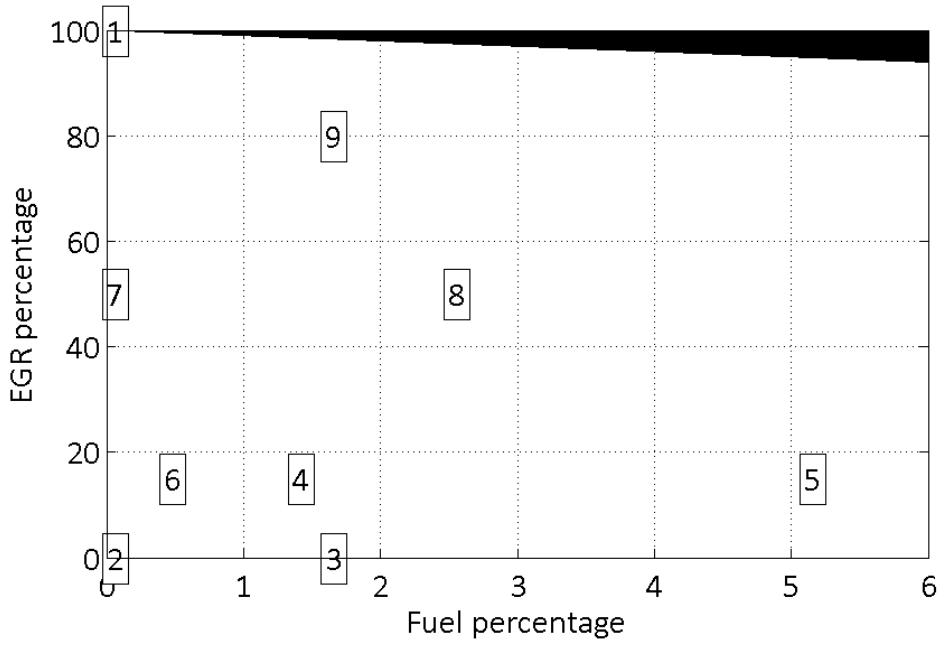

Figure 4.12: *An illustration of the compositions chosen for tests 1-9 as described in table (4.5).*

A theoretical model has been devised in order to simulate the oscillation frequency of LITGS signals measured as a result of different compositions, based on the theory described in section (3.2) and shown in the relevant MATLAB code included in Appendix B. It can be seen from figure (4.13) that the theoretical model accurately predicts the experimental data, and displays good agreement with the

experimentally measured values.

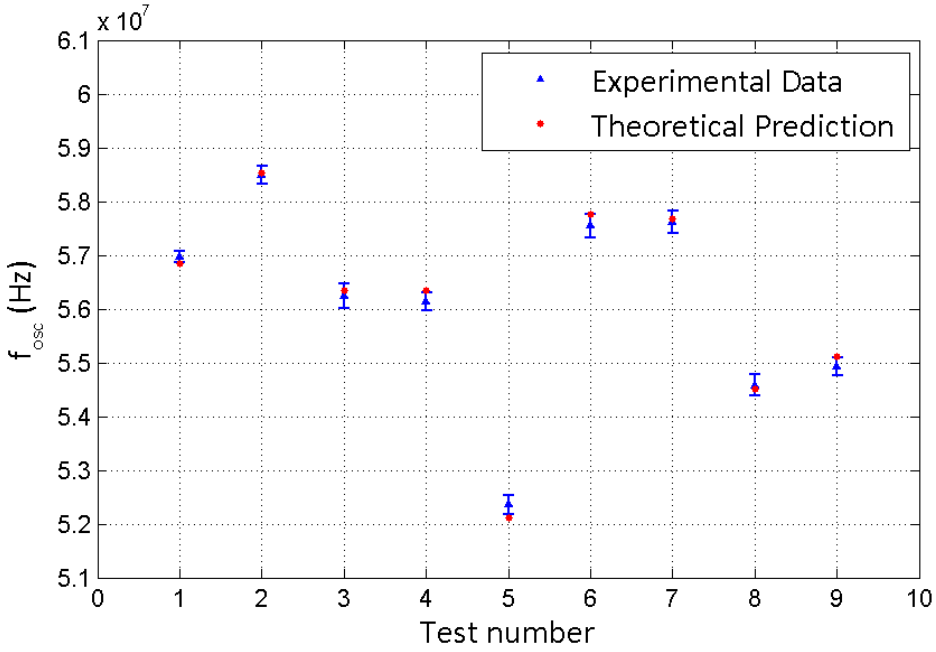

Figure 4.13: *A comparison between the oscillation frequencies determined from the experimental tests of varying composition and the corresponding theoretically calculated values.*

Following this successful test of the model in a more demanding environment where three gases are mixed with fuel vapour, the last step towards verifying the suitability of LITGS for use in IC engine applications was taken.

As previously described, the fundamental source of inaccuracy in temperatures derived from LITGS is uncertainty in composition. Equation (2.6) shows that temperature is linearly proportional to the quantity m/γ. As a result, if a LITGS measurement is taken in an environment where the true m/γ is different from the pre-supposed value, the derived temperature is in error by a fraction corresponding to the fractional difference in m/γ.

Figure (4.14) shows an 'error surface', which was calculated using a MATLAB

code shown in Appendix B. This colour map shows the error in temperature measurement as a function of composition as the mixture of air, fuel and EGR departs from the pre-supposed reference point. In the case of figure (4.14), the reference point is chosen to be at the point marked '4', a composition chosen in analogy to the fourth test described in table (4.5). This composition is of importance because it most closely simulates the mixture of air, fuel and EGR just prior to ignition.

The production of the error surface took the presence of trace species in EGR including Ar, O_2, CO, HC, NO and NO_2 into account, and although these species amount to less than 3 % of a typical EGR composition, these were not accounted for during the experimental tests due to practical difficulties and their small influence on EGR overall.

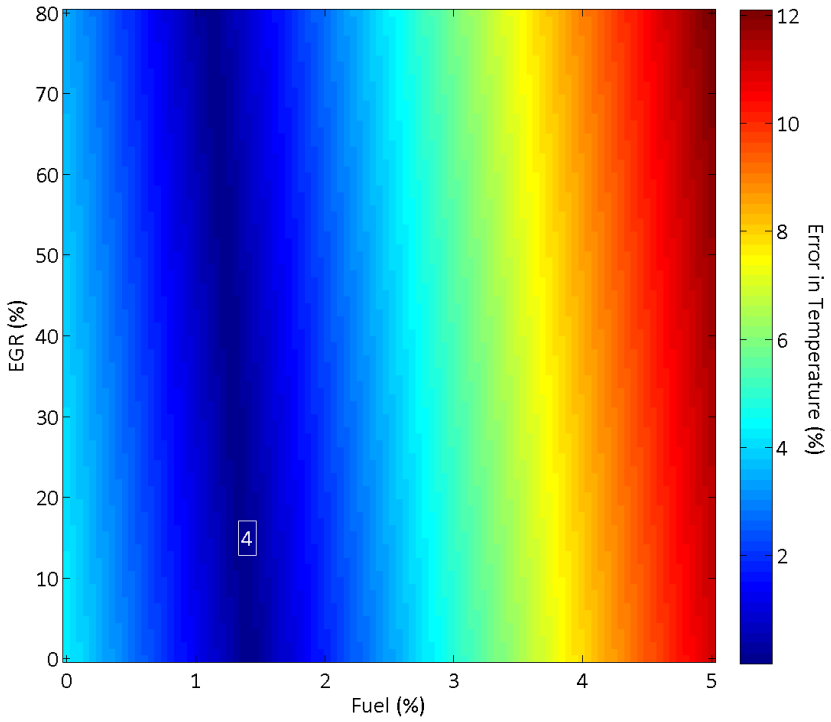

Figure 4.14: *An error surface indicating the error in measurements of temperature within an engine environment resulting from uncertainty in composition.*

The colour-bar to the right side of figure (4.14) allows the error of any composition relative to the reference to be quickly identified. For example, in the event of the actual composition consisting of 3 % fuel and 20 % EGR, the error in the resulting temperature measurement is approximately 4.5 %.

Chapter 5

Discussion of results

Firstly, the benefits of the technique will be summarised and the experimental methods discussed. Secondly, a discussion of the trends displayed in chapter (4) is given in addition to other observations arising from analysis of the LITGS data. Following discussion of the experimental results, the effect of compositional variations on the accuracy of the measurements will be reviewed. Lastly, in terms of continuation of this work, further experiments of interest and potential future work on this topic are discussed, including how this work will influence the design of future experiments.

The requirements of the LITGS technique are that optical access to the measurement location must be available, the incident laser radiation must be absorbed by a species present within the region of interaction of the pump beams and this stored energy must be quenched to allow the production of a density modulation feature that is a grating.

The environment created within an IC engine is hostile, and in the case of optical diagnostics the primary problem is that windows can become coated with by-products of the combustion event. This will affect the intensity of the detected signal. An important attribute of LITGS for use under such conditions is that the measurement of temperature using a LITGS signal is dependent not on intensity

but the frequency of the oscillation. In addition, the high precision of LITGS allows the measurement of subtle effects, making it ideally suited for applications such as the investigation of small changes in composition and temperature.

This work has investigated the effect of compositional variations upon the oscillation frequency of LITGS signals, in order to determine whether the theoretical prediction of the dependence of the oscillation frequency upon the gas composition derived in section (2.2) accurately models the experimental results.

Firstly, a systematic study of varying gas compositions was undertaken at a total pressure of 4 bar and 30°C, focusing on the main components of air and EGR; N_2, O_2 and CO_2. These experiments display an excellent correlation with the expected theoretical fit.

Secondly, these experiments were repeated under the same conditions, with the addition of a saturated vapour of water within the cell. The presence of water introduces a shift to a higher value of γ/m and correspondingly a slightly higher oscillation frequency for each composition as expected, since water has an unusually high value of γ/m. The results of these experiments, displayed in section (4.7), indicate that the effect of this small quantity of water on the oscillation frequency in synthetic EGR is on the borderline of resolution, and continue to show good agreement with the theoretical prediction of the trend.

The final components present in the pre-ignition phase of an engine cycle are varying concentrations of water vapour and fuel. Experiments were conducted in order to verify the theoretical relationship between oscillation frequency and γ/m of these species. The concentrations of water and fuel, iso-octane, were varied in synthetic EGR (containing N_2 and CO_2) and N_2 respectively. The results displayed in sections (4.8) and (4.9) indicate that the theoretical model continues to predict correctly the effect of compositional variations upon the oscillation frequency.

The aim of the final stage of the work is to assess the effect of uncertainty

in gas composition upon the accuracy with which temperature may be measured. Nine tests, each of varying compositions chosen to simulate a possible gas mixture within a region of an engine during the compression stroke, have been conducted and the resulting oscillation frequencies measured. A theoretical model, written in MATLAB, was devised in order to simulate the oscillation frequency of each composition tested. The experimental data display very good agreement with the model prediction, consistently lying within, or very close to, the error bars on the experimental measurements.

Having thoroughly investigated the relationship between oscillation frequency and composition, and having determined that the expected trends are obeyed for all major species, attention was turned to the application of the technique to a real engine environment. An 'error surface', figure (4.14), was constructed in MATLAB based on predictions generated by the validated model, which indicates the magnitude of the error induced in a temperature measurement when composition is not well known in advance.

Based on the results of the error surface, it is clear that fore-knowledge of fuel concentration is significantly more important than that of EGR. In the case of direct-injection engines where the fuel is sprayed directly into the cylinder, localised regions of high fuel concentration are highly likely in the period just subsequent to the injection event. As the cycle progresses, however, these areas of localised high fuel concentration will disappear as turbulent mixing processes affect the cylinder contents. Finally, at the time of ignition, the air/ fuel/ EGR mixture will tend to be most homogeneous, and close to the conditions required for complete combustion (a condition known as 'stoichiometry') [38].

For these reasons, temperatures derived from LITGS should be interpreted most carefully early in the cycle, but they should become increasingly more reliable as the cycle progresses.

The final validation tests shown in this thesis do not include water, owing to the experimental difficulty in evaporating sufficient quantities. An future improvement would be the introduction of a method capable of maintaining the cell and the gas contained within it at temperatures higher than 80°C, enabling the tests to be repeated with the addition of water to the EGR mixture.

The partial pressures of the evaporated liquids have been calculated according to the ideal gas law. Further work could include the adoption of an equation of state accounting for behaviour of real gases, although preliminary calculations using the Van der Waals equation of state resulted in a change in γ/m of less than 1 % for a typical mixture, which is an error that is small when presented on the scale of the figures included in this thesis.

Future work should investigate the possibility of introducing a simple absorption-based measurement of fuel concentration running simultaneously, or attempt to recover some information about fuel concentration from the strengths of the pump beams. Naturally, two line-of-sight measurements do not provide much information about the fuel concentration in the crossing region, but this approach may be sufficient. Another potential avenue to obtaining information concerning fuel concentration is that the strength of a LITGS signal has been shown in the past to be proportional to the amount of absorber in the crossing region. Therefore, integration of a LITGS signal may also provide useful information to limit ignorance about fuel concentration.

Chapter 6

Conclusions

The work contained within this thesis has thoroughly investigated the effect of composition on the oscillation frequency of a LITGS signal, concentrating on the major species that are present in an internal combustion engine environment. A key result of these experiments is the validation of a model which describes the variation in oscillation frequency with composition. This model was then applied to determine the error in LITGS-derived temperature in the case where the composition of gas in the crossing region is allowed to vary in nature, and differs from that of a reference mixture (chosen to match in-cylinder conditions just before ignition).

The understanding imparted by the error surface, figure (4.14), indicates that knowledge of fuel concentration is particularly important in obtaining the most accurate measurements of temperature from the LITGS technique. Whilst total ignorance of the actual fuel concentration could cause errors as large as 12 % (at least, for the conditions shown in figure (4.14)), even a relatively poor estimate of the fuel concentration present may be sufficient to reduce the magnitude of the error considerably. Ultimately, figure (4.14) indicates that a suitable choice of the reference condition against which the temperature measurements are determined in an engine environment, in conjunction with sensible constraints on measurement locality and

timing, will enable LITGS measurements of temperature to be made with an accuracy of approximately 3 %. This corresponds to an error of 10-15 K in 500 K, which at least matches if not beats established techniques, whilst doing so with a much simpler analysis. This will allow the measurement of small temperature changes, such as those due to a phenomenon called 'charge cooling', where evaporating fuel sprays cause a minor drop in in-cylinder gas temperature.

This work provides valuable insights into the accuracy of LITGS as a diagnostic tool with which to measure temperature in engine applications. It will also allow researchers conducting such experiments to make good choices regarding the locations and timings of measurements in order to avoid regions and instants which are likely to result in poor accuracy.

The encouraging nature of the results contained within the body of this thesis indicate that further developments would, however, be worthwhile. The possible operating conditions of this work form a limitation of the study; the maximum temperature and pressure attainable were 80°C and 4 bar respectively.

This limitation has resulted in the ability to include a maximum of around 1 % water vapour in experiments conducted during this work, in comparison with approximately 2 % percent expected to be present in a stoichiometric air-fuel mixture in reality. Such a mixture may be expected to contain around 15 % EGR, 14 % of which is water vapour; for a localised region inside a combustion engine containing pure EGR, water vapour would constitute 14 % of the total composition in that region. Real combustion environments are characterised by temperatures and pressures far exceeding the conditions attainable during the work presented; this would consequently alleviate the limitation on the quantities of water vapour, for example, that could be included in an analogous study within an IC engine. Thus, this study provides an encouraging proof of principle, the next logical step in the development of LITGS as a diagnostic tool for temperature measurement being the application

of this experiment within a real engine environment.

Appendix A: Experimental Record

LITGS: EXPERIMENTAL RECORD

Experiment Date:	
Experiment Number/ Description:	
Pulse Generator Delay:	
Repetition Rate:	
Number of Drops (H_2O):	
Temperature (°C):	

Partial Pressure Increments:	
Total Pressure:	
Gas 1 (initially minority gas):	
Gas 2 (initially majority gas):	
Tracer:	

PREPARATION:

- Turn on lasers → Turn on vacuum pump → Clean/ evacuate cell. Pressure gauge reads -1.000. → Turn on temp. recording feature of oscilloscope ("AUTO USB" displayed on multimeter) → Turn on gas cylinders. Use regulator to raise available pressure of both to 3.2 bar (abs)/ 2.2 bar (gauge).

METHOD:

- Vacuum valve closed, cell valve open → Add minority gas (200 mb CO_2 for READING 2) → Close cell valve.
- Open vacuum valve (evacuate pipes).
- Add majority gas (raise pressure to ambient; 0bar gauge (display "0.050); 1bar absolute).
- Insert tracer (2 drops) → Allow to evaporate → Insert water drop(s) → Allow to evaporate.
- Add majority gas (top up pressure to total; 3bar gauge; 4bar absolute, for example).
- Open laser shutters → "Fill" on oscilloscope (50 shots) → Save.
- Evacuate system. Open vacuum valve → SLOWLY open cell valve until temp. constant.
- Repeat, increasing minority gas according to table below.

EXPERIMENTAL CONDITIONS RECORD:

Test #	Gas 1 (% of Total Pressure)	Gas 1 (CO_2): Pressure		Gas 2 (N_2): Pressure		(4 bar abs.) Total Pressure	
		Absolute	Gauge	Absolute	Gauge	Signal (mV)	Temp (°C)
1	0 %			4000 mb	3000 mb		
2	5 %	200 mb	-0.8 bar	3800 mb	2800 mb		
3	10 %	400 mb	-0.6 bar	3600 mb	2600 mb		
4	15 %	600 mb	-0.4 bar	3400 mb	2400 mb		
5	20 %	800 mb	-0.2 bar	3200 mb	2200 mb		
6	25 %	1000 mb	0 bar	3000 mb	2000 mb		
7	30 %	1200 mb	200 mb	2800 mb	1800 mb		
8	35 %	1400 mb	400 mb	2600 mb	1600 mb		
9	40 %	1600 mb	600 mb	2400 mb	1400 mb		
10	45 %	1800 mb	800 mb	2200 mb	1200 mb		
11	50 %	2000 mb	1000 mb	2000 mb	1000 bar		

NOTES:

Appendix B: MATLAB codes


```
function ReadFiles_v3_f(condition,desc,day)

% Routine to convert LeCroy files into a big .mat
% Ben Williams

dirold=cd;

% Check for the test subdirectory.
% Look for all C4*.dat files in the specified folder.
folder = [condition, '\'];
cd([dirold, '\', folder]);
list=dir('C4*.dat');
cd(dirold);

% Work out the number of the first shot in this folder.
offset = str2double(regexp(list(1).name,['C4' day '(\d+)'],'tokens','once'));

display('Loading folder contents to struct...')

%% Open each file and save details to a structure
for i=1:1:length(list)-1
    j=i+offset-1;
    filestring=[day, num2str(j,'%0.5d'), '.dat'];       % form filestring

    % !!!!!!!!!!!!!!!!!!!!!!!!!!!!!!!!!!!!!!!!!!!!!!!!!!!!!!!!
    % !!! Hardwired for channels 1,2,3,4 being active !!!
    % !!!!!!!!!!!!!!!!!!!!!!!!!!!!!!!!!!!!!!!!!!!!!!!!!!!!!!!!

    if (exist([folder, 'C1', filestring],'file') &&...
            exist([folder, 'C2', filestring],'file') &&...
            exist([folder, 'C3', filestring],'file'))
        T1=load([folder, 'C1', filestring]);
        T2=load([folder, 'C2', filestring]);
        T3=load([folder, 'C3', filestring]);
        T4=load([folder, 'C4', filestring]);

        % Save traces in a cell array
        data.traces{i} = [T1(:,1) T1(:,2) T2(:,2) T3(:,2) T4(:,2)];
        % Save samples per trace
        datalen = length(T4(:,2));
        data.numel(i) = datalen;
        % Save zero offsets per trace based on rough measurement
        data.voffsets(i,:) = [mean(T1(1:round(datalen*0.1),2))...
            0 ... %             mean(T2(1:round(datalen*0.1),2))...
            mean(T3(1:round(datalen*0.1),2))...
            mean(T4(1:round(datalen*0.1),2))];

        % Take some statistics, to use later.
        data.idx(i)=i;
        data.maxes1(i)=max(T1(:,2));
        data.maxes2(i)=max(T2(:,2));
        data.maxes3(i)=max(T3(:,2));
        data.maxes4(i)=max(T4(:,2));

        data.means1(i)=mean(T1(:,2));
```

```
function MakeIA_v2_f(condition)

%% Routine to automatically remove unwanted shots
%% Ben Williams (09/2011).

% Load the desired data set.
load(['output\dataset_', condition, '.mat'])

% Look at a trace half way through, to determine the noise level (first shot
% might be at the wrong vertical gain on the 'scope.
% Search all subsequent traces, to remove anything that doesn't exceed that
% Also cut out anything that exceeds 600mV.

shotnum = round(length(data.traces)/2);
noiseval = max(abs(data.traces{shotnum}(1:round(0.1*data.numel(shotnum)),4)));

%% Find useable traces
% Want signals below a certain value (to avoid saturated
% signals that won't have been recorded properly by the scope).

% Working with channel 3 as signal:
traceval = [data.idx' data.maxes3']; % Concatenate these
traceval2 = flipud(sortrows(traceval,2)); % Sort descending by max value
 go=find(traceval2(:,2)< min(max(data.maxes3), 0.6),1); % Find number of first one↙
that drops below 0.6V...
stop=find(traceval2(:,2)<3*noiseval,1); % ...and first to drop to 3*noiseval
if isempty(stop)
    stop = length(traceval2);
end
interesting=sort(traceval2(go:stop,1))'; % Use the range from go to stop for↙
interesting.
display(['Element ' num2str(go) ' to element ' num2str(stop) ' in range ' num2str↙
(round(min(max(data.maxes3),0.15)*1000)) 'mV to ' num2str(round(3*noiseval*1000),'%↙
3.0f') 'mV'])
display(['Success rate: ' num2str(length(interesting)) '/' num2str(length(traceval))↙
' shots within limits.']);

%% Save the output of this system:
save(['output\autointeresting_', condition, '.mat'],'interesting')

data.interesting = interesting;

save(['output\dataset_', condition, '.mat'],'data')
```

```
%% Script to generate a laser power spectrum from LIGS signal data.
%% Megan Edwards (09/2011).

load output\dataset_tube2.mat

%% Create data to analyse

Fs = 5e9;              % Sampling frequency (Hz)
T = 1/Fs;                      % Sample time (s)
L = 5002;                      % Length of signal
t = (0:L-1)*T;                 % Time vector

% Choose a data set to analyse:
y = data.traces{26}(:,4);

figure(1)
subplot(2,1,1)

% PLOT THE SIGNAL VARIATION AS A FUNCTION OF TIME:
h1 = plot(Fs*t(1:end),y(1:end));
h3 = title('Variation in LITGS signal intensity with time');
h4 = xlabel('Time (ms)');
h5 = ylabel('Signal');
axis([0,5000,-0.05,0.15])

%% Compute Power Spectrum

NFFT = 2^nextpow2(L); % Next power of 2 from length of y
Y = fft(y,NFFT)/L;
f = Fs/2*linspace(0,1,NFFT/2+1);

figure(1)
subplot(2,1,2)

% PLOT single-sided amplitude spectrum.
h2 = plot(f,2*abs(Y(1:NFFT/2+1)));
h6 = title('Amplitude Spectrum');
h7 = xlabel('Frequency (Hz)');
h8 = ylabel('|Y(f)|');

axis([0,5e8,0,0.01]);

set([h3 h4 h5 h6 h7 h8],'FontName','Calibri','FontSize',11);
set(gca,'FontName','Calibri','FontSize',11);
grid on

set([h1 h2],'LineWidth',1.5)
%set([h1 h2],'LineWidth',1)
%set([h1 h2],'MarkerSize',10)

set(gca,'LineWidth',0.5,'Box','on')

set(gcf, 'PaperPositionMode', 'manual');
set(gcf, 'PaperUnits', 'centimeters');
set(gcf, 'PaperType', 'A4');
```

```
%% "ProcWrapper" code used to call all functions and codes used during the
%% data analysis procedure.
%% Ben Williams, Megan Edwards (09/2011).

% Clear the workspace:
clear; clc;

% Enter the composition-specific variables (molecular mass (m), ratio of specific↙
heats (g) and total pressure (pt):
day = 'litgs';
desc = '110829';
m1 = 44;
m2 = 32;
m3 = 28;
g1 = 1.3;
g2 = 1.4;
g3 = 1.404;
pt = 4000;

%% Load the raw data files for the experiments considered:
types = [{'0-800-3200'},{'200-600-3200'},{'400-400-3200'},{'600-200-3200(2)'},{'800-↙
0-3200'}];

% Ensure that the output directory exists:
if ~exist('output','dir')
    mkdir('output')
end

% Keep a note of the initial directory:
dirold=cd;

diary(['diary_' desc '_' datestr(now,'yymmdd-HHMM') '.txt'])

% Iteratively cycle through all data sets and apply each code used during the data↙
analysis procedure:

for k=1:length(types)

    display(' ')
    display(['Attempting to load "' types{k} '" test data.']);
    display(['Attempting to load "' types{k} '" O-N.']);

    % Check that the test type exists, then open the file:
    if exist(types{k},'dir')
        % Load all of the raw data (from the oscilloscope) for a given subfolder:
        display(['Opening ' dirold, '\', types{k}, '...']);
        ReadFiles_v3_f(types{k},desc,day)

        % Display a warning if a folder is not found (ie. misnamed):
    else display('Cannot find folder')

    end

    if exist(['output\dataset_' types{k} '.mat'],'file')
        % Automatically reject poor shots:
```

```
%% CODE TO PLOT THE EXPERIMENTAL OSCILLATION FREQUENCY vs. gamma/m AND TO COMPARE TO↙
THE THEORETICAL FIT (Derived from kinetics).

function [TheoreticalFit x y error] = fitting_oscfrq(m1,m2,m3,g1,g2,g3,pp1,pp2,pp3,↙
PT,Oscillation_Frequencies,error)

% Working with figure 1 specifically...
figure(1);
% blank figure and reset parameters:
clf reset

% Input experimental data; values for the molecular mass and ratio of specific heats↙
of each species are defined in the code "ProcWrapper.m":
% Weighted mean molecular mass and ratio of specific heats (gamma) for each↙
composition:
Molecular_Masses = m1*((pp1)/PT) + m2*(pp2/PT) + m3*(pp3/PT);
Gammas = g1*((pp1)/PT) + g2*(pp2/PT) +g3*(pp3/PT);

% Define the x and y axes data:
x = Gammas./Molecular_Masses;
y = Oscillation_Frequencies;

% Calculate the theoretical fit to the data
TheoreticalFit = polyfit(sqrt(x),y,1); % fit like y=m*sqrt(x)+c

% Plot the experimental data:
h1=errorbar(x,y,error,'.');

% Plot the theoretical fit line:
h3=line(x,TheoreticalFit(1)*sqrt(x)+ TheoreticalFit(2),'Color','red');

% Label the axes:
h4 = xlabel('\gamma/ m (mol/g)');
h5 = ylabel('f_o_s_c (Hz)');

display(['Fit with gradient: ' num2str(TheoreticalFit(1),3) ' and intercept: '↙
num2str(TheoreticalFit(2),3)]);

hold off

errorbar_tick(h1,80);

%% Designate the aesthetics of the plot:
set([h4 h5],'FontName','Calibri','FontSize',11);
set(gca,'FontName','Calibri','FontSize',11);
grid on

set(h3,'LineWidth',1.5)
set(h1,'LineWidth',1)
set(h1,'MarkerSize',10)

set(gca,'LineWidth',0.5,'Box','on')

set(gcf, 'PaperPositionMode', 'manual');
```

```
%% Routine to Plot Theoretical vs. Experimental Data.
%% Megan Edwards (September 2011).

%% Load both the theoretical and experimental data matrices:
load '..\110909 - C8H18-O2-CO2-N2\110909H2O_fitxyerror.mat'
expt = [x;y;error];

load '..\110909 - C8H18-O2-CO2-N2\110909THEORY_fitxyerror.mat'
theory = [x;y];


figure(2)
clf reset

%% Plot the experimental oscillation frequencies (h1) and the theoretical predictions↙
(h2):

hold on
h1 = errorbar(expt(1,:),expt(2,:),expt(3,:),'b^');
h2 = plot(theory(1,:),theory(2,:),'r.');
hold off

h4 = xlabel('Test Number');
h5 = ylabel('f_o_s_c (Hz)');
h6 = legend([h1 h2],'Experimental data','Theoretical model','Location','NW');

axis([0,10,5.1e7,6.1e7]);

%% Designate the aesthetics of the plot.

errorbar_tick(h1,80);

set([h4 h5 h6],'FontName','Calibri','FontSize',11);
set(gca,'FontName','Calibri','FontSize',11);
grid on

set([h1 h2],'LineWidth',1)
set([h1 h2],'MarkerSize',10)

set(gca,'LineWidth',0.5,'Box','on')

set(h1, 'MarkerFaceColor', 'b', 'MarkerSize', 3);
set(gcf, 'PaperPositionMode', 'manual');
set(gcf, 'PaperUnits', 'centimeters');
set(gcf, 'PaperType', 'A4');
set(gcf, 'PaperPosition', [2 17.68 16 10]);
set(gcf, 'PaperOrientation','portrait');

%% Save the plot in a format convenient to import to LaTeX:

saveas(gcf,'110909 - VaryingTests_comparison.fig')
saveas(gcf,'110909 - VaryingTests_comparison.png')
```

```
%% Theoretical Prediction for Tests of Varying Compositions.
%% Megan Edwards (September 2011).

% Aim: to predict the oscillation frequency for each of the 9 tests, each
% of a different gas-fuel composition.

% Method: 1). Calculate fringe spacing, 2).Calculate the speed of sound, cs,
% 4). Calculate f_(osc).

clc;clear

%% Crossing angle of pump beams and fringe spacing.

Spacing = 6.41e-6;

%% The ratio 'gamma/m' for each test is denoted ratio1-ratio9.

%Molecular masses for all five species (kg):
m1 = 44e-3/6.023e23; % Carbon dioxide
m2 = 32e-3/6.023e23; % Oxygen
m3 = 28e-3/6.023e23; % Nitrogen
m4 = 114e-3/6.023e23; % Iso-octane
m5 = 58.08e-3/6.023e23; % Acetone

%Ratio of specific heats for all five species:
g1 = 1.3; % Carbon dioxide
g2 = 1.4; % Oxygen
g3 = 1.404; % Nitrogen
g4 = 1.02; % Iso-octane
g5 = 1.11; % Acetone

% Gamma/m will vary for each of the 9 tests (imported from Excel file):

ratio1 = 2.72448E+25;
ratio2 = 2.88847E+25;
ratio3 = 2.67724E+25;
ratio4 = 2.67656E+25;
ratio5 = 2.29002E+25;
ratio6 = 2.81354E+25;
ratio7 = 2.80449E+25;
ratio8 = 2.50544E+25;
ratio9 = 2.56186E+25;

%% The speed of sound (cs) depends upon gamma, m, T, Boltzmann's constant.

T = 80+273.15; % (K)
kB = 1.38e-23; % (m^2 kg s^-2 K^-1)

% The speed of sound will vary for each test:

cs1 = sqrt(ratio1*kB*T);
cs2 = sqrt(ratio2*kB*T);
cs3 = sqrt(ratio3*kB*T);
cs4 = sqrt(ratio4*kB*T);
cs5 = sqrt(ratio5*kB*T);
```

```
%% Code to plot an error surface for temperature vs. composition

%% Input the species variables.

% Input the mean (weighted) molecular masses of air, EGR and fuel.
mAIR = 28.9732;
mEGR = 28.76923;
mFUEL = 114; %C8H18

% Input the mean (weighted) ratios of the ratios of specific heat of air, EGR and↙
fuel.
gAIR = 1.40621;
gEGR = 1.38107;
gFUEL = 1.08; %C8H18

% Generate linearly spaced vectors for both the fuel and EGR axes.
steps = 100;
fuels = linspace(0,5,steps);
EGRs = linspace(0,80,steps);

% Generate an array each for fuel (FM) and EGR (EM), for a 3D plot.
[FM EM] = meshgrid(fuels, EGRs);

% Average mass and gamma at each individual point in the combined matrices:
mass_matx = FM*mFUEL+EM*mEGR+(100-FM-EM)*mAIR;
gamma_matx = FM*gFUEL+EM*gEGR+(100-FM-EM)*gAIR;

ratio_matx = mass_matx./gamma_matx; %m/gamma

% Set parameters for reference point (Test 4).
fuel_pc = 1.36;
EGR_pc = 15;
% The percentage of air is equal to 100 minus that of both EGR and fuel.
air_pc = 100-fuel_pc-EGR_pc;

% Average mass and gamma for the reference point.
mass_ref = (fuel_pc*mFUEL+EGR_pc*mEGR+air_pc*mAIR);
gamma_ref = (fuel_pc*gFUEL+EGR_pc*gEGR+air_pc*gAIR);

ratio_ref = mass_ref/gamma_ref; %m/gamma

% Fractional change in m/gamma of every combination (fuel, EGR) wrt. reference point.
deviation_matx = 100*abs(ratio_matx - ratio_ref)/ratio_ref;

figure(3)

clf reset

% 'imagesc' displays the colour map image.
imagesc(fuels,EGRs,(deviation_matx))

% Label axes:
h1 = xlabel('Fuel (%)');
h2 = ylabel('EGR (%)');
```

Bibliography

[1] M. Asif et al., *Energy supply, its demand and security issues for developed and emerging economies* Renewable and Sustainable Energy Reviews, 11, 1388-1413, 2007.

[2] T. Thielemann et al., *Lignite and hard coal: Energy suppliers for world needs until the year 2100 An outlook*, International Journal of Coal Geology, 72, 1-14, 2007.

[3] Shahriar Shafiee and Erkan Topal, *When will fossil fuel reserves be diminished?*, Energy Policy, 37, 181-189, 2009.

[4] EC. Regulation 715/2007, *Euro 5 and Euro 6 standards*, 2007.

[5] E. B. Cummings, *Laser-induced thermal acoustics: simple accurate gas measurements*, Optics Letters, 19 (17), 1361-1363, 1994.

[6] H. J. Eichler, P. Günter and D. W. Pohl, *Laser Induced Dynamic Gratings*, Springer, Berlin, 1986.

[7] D. C. Auth, *New high-power source of coherent microwave phonons*, Appl. Phys. Lett., 16, 512, 1970.

[8] Philip H. Paul, Roger L. Farrow and Paul M. Danehy, *Gas-phase thermal-grating contributions to four-wave mixing*, J. Opt. Soc. Am. B., 12 (3), 384, 1995.

[9] A. Stampanoni-Panariello, D. N. Kozlov, P. P. Radi, B. Hemmerling, *Gas-phase diagnostics by laser-induced gratings I. theory*, Appl. Phys. B., 81, 101, 2005.

[10] A. Dreizler, T. Dreier, J. Wolfrum, *Thermal grating effects in infrared degenerate four-wave mixing for trace gas detection*, Chem. Phys. Lett, 233, 525-532, 1995.

[11] E. B. Cummings, I. A. Leyva and H. G. Hornung, *Laser-induced thermal acoustics (LITA) signals from finite beams*, Applied Optics, 34 (18), 3290-3302, 1995.

[12] D. J. W. Walker, R. B. Williams and P. Ewart, *Thermal Grating Velocimetry*, Opt. Lett, 23 (16), 1316, 1998.

[13] B. Hemmerling, R. Bombach, W. Hubschmid, *Laser-induced gratings in oxygen excited via the b* $^1\Sigma_g^+$ *(v' = 0) state*, Chem. Phys. Lett, 256, 71-76, 1996.

[14] S. Williams, L. A. Rahn, P. H. Paul, J. W. Forsman and R. N. Zare, *Laser-induced thermal grating effects in flames*, Opt. Lett, 19 (21), 1681, 1994.

[15] H. Latzel, A. Dreizler, T. Dreier, J. Heinze, M. Dillmann, W. Stricker, G. M. Lloyd and P. Ewart, *Thermal grating and broadband degenerate four-wave mixing spectroscopy of OH in high-pressure flames*, Appl. Phys. B, 67, 667-673, 1998.

[16] R. Stevens and P. Ewart, *Single-shot measurement of temperature and pressure using laser-induced thermal gratings with a long probe pulse*, Appl. Phys. B, 78, 111-117, 2004.

[17] R. E. Stevens, *Laser-Induced Grating Techniques for Combustion Diagnostics*, DPhil Thesis, University of Oxford, 2004.

[18] A. Stampanoni-Panariello, D. N. Kozlov, P. P. Radi, B. Hemmerling, *Gas-phase diagnostics by laser-induced gratings II. Experiments*, Appl. Phys. B., 81, 113-129, 2005.

[19] M. Gutfleisch, D. I. Shin, T. Dreier, P. M. Danehy, *Mid-infrared laser-induced grating experiments of C_2H_4 and NH_3 from 0.1-2 MPa and 300-800 K*, Appl. Phys. B., 71, 673-680, 2000.

[20] E. B. Cummings, H. G. Hornung, M. S. Brown and P. A. DeBarber, *Measurement of gas-phase sound speed and thermal diffusivity over a broad pressure range using laser-induced thermal acoustics*, Opt. Lett, 20 (14), 1577, 1995.

[21] E. F. McCormack, S. T. Pratt, P. M. Dehmer and J. L. Dehmer, *Double-resonance laser-induced grating spectroscopy of nitric oxide*, Chem. Phys. Lett., 211 (1), 147-155, 1993.

[22] J. A. Booze, D. E. Govoni and F. F. Crim, *Diffraction mechanisms in gas-phase laser induced grating spectroscopy of vibrational overtone transitions*, J. Chem. Phys., 103 (24), 10484-10488, 1995.

[23] B. Hemmerling, D. N. Kozlov, O. M. Stel'makh and B. Attal-Tretout, *Diagnostics of water-containing gas mixtures using thermal laser-induced gratings*, Chemical Physics, 320, 103-117, 2006.

[24] M. S. Brown and W. L. Roberts, *Single-Point Thermometry in High-Pressure, Sooting, Premixed Combustion Environments*, J. Propuls. Power, 15 (6), 119-127, 1999.

[25] R. C. Hart, G. C. Herring and R. J. Balla, *Pressure measurement in supersonic air flow by differential absorptive laser-induced thermal acoustics*, Optics Letters., 32 (12), 1689-1691, 2007.

[26] Keith A. Nelson, D. R. Lutz, M. D. Fayer and Larry Madison, *Laser-induced phonon spectroscopy. Optical generation of ultrasonic waves and investigation of electronic excited-state interactions in solids*, Phys. Rev. B., 24(6), 3261, 1981.

[27] W. Hubschmid, B. Hemmerling and A. Stampanoni-Panariello, *Rayleigh and Brillouin modes in electrostrictive gratings*, J. Opt. Soc. Am. B, 12 (10), 1850-1854, 1995.

[28] A. Stampanoni-Panariello, *Laser-Induced Gratings in the Gas Phase: Formation Mechanisms and Applications for Diagnostics*, ETH Zurich, Doctoral Thesis, 2003.

[29] A. Stampanoni- Panariello, D. N. Kozlov, P. P. Radi, B. Hemmerling, *Gas phase diagnostics by laser-induced gratings I. theory*, Appl. Phys. B, 81, 101-111, 2005.

[30] Johannes Kiefer and Paul Ewart, *Laser diagnostics and minor species detection in combustion using resonant four-wave mixing*, Progress in Energy and Combustion Science, 2010.

[31] Stephen J. Blundell and Katherine M. Blundell, *Concepts in Thermal Physics*, Oxford University Press, 2006.

[32] M. C. J. Coolen, R. N. Kieft, C. C. M. Rindt and A. A. van Steenhoven, *Application of 2-D LIF temperature measurements in water using a Nd:YAG laser*, Experiments in Fluids, 27, 420-426, 1999.

[33] X. Pan, P. F. Barker, A. Meschanov, J. H. Grinstead, M. N. Schneider and R. B. Miles, *Temperature measurements by coherent Rayleigh scattering*, Optics Letters, 27 (3), 161-163, 1999.

[34] F. Zhao and H. Hiroyasu, *The application of laser-Rayleigh scattering to combustion diagnostics*, Progress in Energy and Combustion Science, 19, 447-485, 1993.

[35] Thomas Seeger and Alfred Leipertz, *Experimental comparison of single-shot broadband vibrational and dual-broadband pure rotational coherent anti-Stokes Raman scattering in hot air.*, Applied Optics, 35 (15), 2665-2671, 1996.

[36] Thomas Dreier and Paul Ewart, *Coherent Techniques for Measurements with Intermediate Concentrations.*, Applied Combustion Diagnostics (Edited by K. Kohse-Höinghaus and J. B. Jeffries), 35 (15), 69-811, 1996.

[37] D. R. Snelling, R. A. Sawchuck and T. Parameswaran, *Noise in single-shot broadband coherent anti-Stokes Raman spectroscopy that employs a modeless dye laser.*, Applied Optics, 33 (36), 8295-8301, 1994.

[38] Benjamin A. O. Williams, *Quantitative Laser Diagnostics for Combustion*, DPhil Thesis, University of Oxford, 2009.

[39] Continuum Electro-Optics, Inc, *Minilite Operation Manual*, 3150 Central Expressway, Santa Clara, CA 95051, 1997.

[40] R. Stone, *Introduction to Internal Combustion Engines*, Third edition, Macmillan Press Ltd., 1999.

[41] National Institute of Standards and Technology, *NIST Chemistry Webbook*, http://webbook.nist.gov/, 2009.